

## Authors' Response to Comments

2

3 M. S. Johnson (Referee)

4 msj@kiku.dk

5 Received and published: 13 October 2014

## 6 Review of: SO<sub>2</sub> photolysis as a source for sulfur mass-independent isotope signatures

7 in stratospheric aerosols by Whitehill, Jiang, Guo and Ono

8

9 *This paper describes a series of experiments into the S-MIF pattern produced by SO<sub>2</sub>*  
10 *photochemistry, with emphasis on photolysis. It is asserted that SO<sub>2</sub> photolysis is*  
11 *responsible for the S-MIF signal observed in some volcanic sulfate in polar ice cores*  
12 *because some of the SO photoproduct combines with O<sub>2</sub> in the atmosphere in a three*  
13 *body reaction to form SO<sub>3</sub> which reacts with H<sub>2</sub>O to produce H<sub>2</sub>SO<sub>4</sub>. The rate of this*  
14 *reaction is poorly constrained (the only evidence is one determination in the literature*  
15 *of an upper limit) and an effort is made to estimate it's rate. Stationary points on*  
16 *the SO<sub>3</sub> potential energy surface are investigated using quantum chemistry, and a*  
17 *chemical box model is used to interpret the experimental results. The paper describes*  
18 *a well-designed set of experiments and painstaking isotopic analysis. There is a lot*  
19 *of interesting material here that makes it a pleasure to read and a valuable addition*  
20 *to the field. I have a few concerns detailed below that should be addressed prior to*  
21 *publication.*

22

## 23 *Scientific comments*

24 *The Introduction is very well written and gives a readable review of current understanding*  
25 *in the field. In 23501, 23 (page, line) it is stated that the experimentally measured*

1    1% KIE for  $34SO_2$  reaction with OH relative to  $32SO_2$  is incompatible with Castleman's  
2    measurement of 1974. First, note that this is a single measurement 40 years  
3    ago, good work but it includes some uncertainty. More importantly, the experimental  
4    measurement was done in the range of -20 to +40 C and does not include the temperature  
5    at which the  $SO_2 + OH$  oxidation took place high in the atmosphere. One must  
6    extrapolate the measured KIEs outside the range of the study without a reason to think  
7    the temperature dependence of the KIE would be linear. Overall, given these issues, it  
8    is speculative to say the experiment and the field measurement do not agree. Suggest  
9    more cautious language - perhaps there is an indication, but nothing as clear cut as  
10   the text appears to claim.

11

12    Changed to more cautious wording.

13

14    There must be some water in the photoreactor, in order to convert  $SO_3$  into  $H_2SO_4$ .  
15    There is always some water on anything that has been open to the atmosphere, including  
16    anything that has not been pumped out under high vacuum for many days. How  
17    much water? Was OH produced via water photolysis or  $O(1D)$  plus  $H_2O$ ?

18

19    Added section discussing water and added  $HO_x$  chemistry to photochemical model

20

21    23500, 27, why 'requires a high  $SO_2$  column density'? Not clearly argued in the  
22    text. Please discuss how 'requires' is meant - does this mean a large amount of  
23     $SO_2$  between the place where  $SO_2$  is photolysed and the sun, in order to ensure  
24    self-shielding? Or, simply that there is enough  $SO_2$  present in a plume to ensure a  
25    signal?

26

1    Changed to be more specific

2

3    *23500, 27, why 'an SO<sub>2</sub> plume reaching an altitude of 25 km or higher'? This limit*  
4    *seems somewhat arbitrary. According to Figure 8, 20 km should be sufficient. Including*  
5    *uncertainties, could it not simply say, 'above the tropopause'?*

6

7    Changed to "around 20 to 25 km". The exact altitude depends on atmospheric conditions and  
8    requires modeling beyond the scope of the present paper.

9

10    *For example at 23514, 12. Isotope selective intersystem crossing due to an accidental*  
11    *near degeneracy is a plausible theory with some evidence to back it up. It is an advance*  
12    *to the field. However, it will act at the same time as other mechanisms including selfshielding*  
13    *and the rate of photoabsorption (isotopologue-dependent cross section), not*  
14    *instead of them. The overall effect will be a combination of the basic mechanisms.*

15

16    Clarified this section to make it clear that optical isotope effects (i.e. cross-section differences  
17    and self-shielding) are also present. Optical isotope effects are definitely important in both  
18    absorption regions, but (as shown in Whitehill et al. 2013) cannot explain the entirety of the  
19    mass-independent isotope effect in the 250 to 350 nm region.

20

21    *Section 4.2. The 'Ran-Lyon' model uses isotope-dependent vibrational frequencies to*  
22    *derive shifts, and the isotopologue-dependent absorption cross sections are obtained*  
23    *as shifted versions of the 32SO<sub>2</sub> absorption cross section. This approach does not*  
24    *take into account changes in the Franck-Condon factors observed by Danielache et*  
25    *al., or changes in the rotational constants/rotational fine structure. This is important*  
26    *when calculating self-shielding. The agreement with experiment is fine, but keep in*  
27    *mind there is more to the story and the model may have gotten the right answer for the*

1 wrong reasons.

2

3 Reworded this section to make it clear that the “Ran-Lyons” model is not accurate. However,  
4 it produces reasonable results comparable with experimental data (under some conditions)  
5 and thus provide a useful tool until better cross-sections at appropriate temperatures are  
6 available.

7

8 *The model and the discussion do not consider HOx chemistry, and they do not consider*  
9 *photochemistry of the reduced sulfur compounds. Polysulfur product is extracted and*  
10 *analyzed, and so some additional reactions must take place:  $S + S_2 + M \rightarrow S_3 + M$ ;*  
11 *oxidation of reduced sulfur, photolysis of polysulfur species, etc. Any of them could*  
12 *reasonably*

13 *give S-MIF in analogy to the oxygen reactions (for example ozone formation,*  
14 *ozone photolysis, etc.).*

15

16 Added HOx chemistry and polysulfur chemistry (up through  $S_2$ ) to the kinetic model.

17

18 Although we have no constraints on water within the system, HOx chemistry does not cause a  
19 major difference in the results at reasonable estimates of water (< 100 ppm). Addition of  
20 more water increases the estimated rate constant, so it is consistent with our attempts to find a  
21 lower bound on the rate.

22

23 Under the conditions tested here (5% - 20% oxygen in nitrogen), the model predicts that S  
24 and  $S_2$  will be insignificant species, with steady state concentrations of  $\sim 100$  molecules  $\text{cm}^{-3}$   
25 (for S) and  $\sim 10^{-8}$  molecules  $\text{cm}^{-3}$  (for  $S_2$ ). Therefore, reaction between S and  $S_2$  will not be  
26 significant in the presence of oxygen. This is consistent with the lack of elemental sulfur  
27 products recovered in all experiments performed in the presence of  $\text{O}_2$ .

28

1    In Figure 6, for the no oxygen case, why don't the sulfate and  
2    the elemental sulfur show mass balance of the isotopes, equal and opposite D33S? If  
3    SO<sub>2</sub> photolysis is the source of both S<sub>n</sub> (polysulfur) and sulfate, why don't they have  
4    the same D33S?

5  
6    The mass-balance is satisfied by the residual SO<sub>2</sub>, which probably carries a negative D33S  
7    value. In these open system experiments, in the absence of oxygen, both S<sub>n</sub> and sulfate  
8    carry positive D33S values. This is consistent with previous experiments in the literature (e.g.  
9    Ono et al. 2013 shows both sulfate and elemental sulfur with positive D33S values). They do  
10   not have the same D33S values because, in the absence of O<sub>2</sub>, most of the sulfate comes from  
11   SO<sub>2</sub> + O or SO<sub>2</sub> + OH reactions rather than SO<sub>2</sub> photolysis, as discussed in Section 4.3.

12  
13   Is equation (7) for the spectral irradiance of the lamp independent of the distance from  
14   the lamp? What is the uncertainty in this empirical equation?

15  
16   The distance between the cell and the lamp has a minor effect on the spectral irradiance of the  
17   lamp due to the absorption of oxygen (and some ozone). A brief section is added  
18   acknowledging this. Previous studies (Whitehill and Ono 2012) using a similar lamp tested  
19   the effects and found that they are important below about 195 nm, but relatively insignificant  
20   (in terms of total SO<sub>2</sub> photolysis rates) at long wavelengths.

21  
22   Unfortunately, the empirical expression is fit from the manufacturer's data and the uncertainty  
23   in the measurement is not available. We guess that it is sufficient to estimate the SO<sub>2</sub>  
24   photolysis rate to within an order of magnitude or better, but it is impossible to know without  
25   measuring it. Uncertainty in the lamp is discussed in Section 4.3 (although a quantitative  
26   estimate is not given).

27  
28   23522, 7, Tunneling of oxygen and/or sulfur should not have any effect at all on the  
29   rates of these reactions. Please omit this throw-away explanation.

1  
2 We omitted this explanation.  
3  
4 23522, 27, on the fly transition state hopping calculations would ('in theory') be able to  
5 derive rate constants without the need for global PESs.  
6  
7 Added a sentence acknowledging the potential of on the fly transition state hopping  
8 calculations. Performing such calculations is beyond the scope of this paper.  
9  
10 *Section 4.6. First: Three body reactions get faster as temperature decreases. What is*  
11 *the temperature dependence of R6? Second: The discussion in this section ignores*  
12 *the potential role of photoexcitation – the light flux in the photoexcitation range is much*  
13 *larger than in the photodissociation range. Please include and discuss.*  
14  
15 The temperature dependence of R6 is beyond the scope of the present work. Added a  
16 paragraph in Section 4.7 addressing possible contributions of photoexcitation to the isotope  
17 signatures.  
18  
19 23525, 20, *Since the Lyons results are do not give accurate high resolution rovibronic*  
20 *structure, how can they give an accurate prediction of self-shielding? The rotational*  
21 *fine structure is very important for self-shielding.*  
22  
23 Removed statement that Lyons results predict results accurately.  
24  
25 23526, *section 4.7, given the actinic flux spectrum and the SO<sub>2</sub> absorption spectrum,*  
26 *it is beyond doubt that photoexcitation will take place. This process very likely has an*

1 isotopic signature. What is there to say that photoexcitation and photodissociation do  
2 not occur simultaneously?

3  
4 Section 4.7 attempts to argue that SO<sub>2</sub>photoexcitation alone is not responsible for the  
5 anomalous isotope effects and that SO<sub>2</sub> photolysis is important as well. Added a paragraph  
6 acknowledging the possible contributions from photoexcitation.

7  
8 In Table 2, why is there such a large difference between the values obtained in the first  
9 and second experiment at each temperature? In each case there is a significant drop  
10 in d33S, d34S, d36S. Please discuss. Could S chemistry play a role?

11  
12 We added a section (Section 4.8 in the revised manuscript) that addresses caveats with the  
13 experimental studies and discusses possible sources of variability between duplicate  
14 experiments.

15  
16 Table 3, do the organosulfur product enrichments match the predictions of Danielache  
17 et al.?

18  
19 The results from Table 3 (at lower temperature) cannot be directly compared to the room-  
20 temperature measurements of Danielache et al. (2012). Room-temperature experiments under  
21 similar conditions are compared to room-temperature cross-sections in a previous publication  
22 (Whitehill et al. 2013).

23  
24 Table 4, it is suspicious that there is a negative trend in  $k(R6)$  as the oxygen pressure  
25 increases. The model includes O<sub>2</sub> pressure and Ox chemistry, so in theory, this trend  
26 should not be here. Why is the result so dependent on pO<sub>2</sub>?

27

1 k(R6) results in Table 4 come from the rate estimates in Section 4.3, so they do not explicitly  
2 include Ox chemistry. They include only total product formation rate and estimated fraction  
3 of product formation from R6 (based on D33S values). In our opinion, the values calculated  
4 for  $pO_2 = 5, 10, 15$  kPa are all similar ( $\sim 1e-37$ ), and it is only at 19.8 kPa that a decrease is  
5 observed. This behavior could be due to  $H_2O$  limitation on sulfate aerosol formation at higher  
6  $SO_3$  formation rates (i.e. higher  $O_2$  pressures), but this is purely speculative.

7  
8 *Table 5, why are the two runs with each filter (200BP, 250LP) so different in terms of*  
9 *delta values? Please explain.*

10  
11 The two 200BP experiments were performed at very different conditions (300 kPa  $SO_2$  versus  
12 50 kPa  $SO_2$ ) and that likely explains the discrepancy. The two 250 LP experiments are  
13 performed under identical conditions, and yet yields are different by an order of magnitude  
14 and isotopic composition is different by a factor of 2. The photoexcitation experiments are  
15 challenging and have a very low sulfate formation rate. Additional experiments should be  
16 performed to clarify the results from photoexcitation experiments, but is beyond the scope of  
17 the present paper.

18  
19 *Table 6. The quantum chemistry results are used to make qualitative arguments and*  
20 *the level of calculations does seem adequate to this task. However, as seen here and*  
21 *in tables 7 and 8, the energies obtained using the different methods are very different.*  
22 *How should we know which one to believe, and is there any way to know that the*  
23 *ultimate method used in this paper is adequate to the task? What are the error bars on*  
24 *the resulting values?*

25  
26 It is true that the energies obtained using different methods are different, implying the  
27 difficulties dealing with this challenging system by ab-initio calculations. Among those ab-  
28 initio methods used in this work, UCCSD(T) energies should be the most trustworthy based  
29 on comparison with asymptotic values and thermodynamic data in Section 3.3. Given the

1 multi-reference feature and non-adiabatic coupling involved in multiple electronic states of  
2  $\text{SO}_3$ , however, an ultimately definitive evaluation of the reaction profile would need further  
3 higher level treatment which is beyond the scope of this paper.

4

5 *Table 9, I do not see sulfate formation. How much water is there? What are the*  
6 *concentrations of the HOx radicals?*

7

8 The model was modified to include HOx chemistry. We found that inclusion of  
9  $\text{H}_2\text{SO}_4$  aerosol formation significantly underestimated total product formation for reasonable  
10 values of  $\text{H}_2\text{O}$ , thus suggesting that condensation of  $\text{SO}_3$  on the walls of the cell or other  
11 aerosol particles might be an important process. Modelling this is beyond the scope of the  
12 present paper. Therefore, we focused on the rate of  $\text{SO}_3$  formation from different pathways.

13

14 *Figure 1. Very nice straight line. Does this need to be included, and as Figure 1?*

15

16 Inclusion of temperature calibration is important for demonstrating that our experiments are  
17 robust and that we are testing what we claim to be testing.

18

19 *Perhaps it could be put in a supplementary information file, or better yet, left out. The*  
20 *equation and a short description are all that is needed.*

21 *Figure 3, very nice result.*

22 *Figure 7, left. The model always predicts increased  $f_{\text{R}6}$  as  $\text{O}_2$  is increased, yet this*  
23 *is not observed in the experiments. Do you have an explanation? Why should we*  
24 *have believe the model and the resulting rate? The rate is not determined directly, but*  
25 *indirectly, via the model. This introduces many uncertainties (J value, completeness of*  
26 *model), and this difference is yet another indication that the model is not right. (The*  
27 *first, as noted above, was that the value of  $k$  varies with the oxygen content).*

1  
2 Our revised model also predicts increased f\_R6 values as O<sub>2</sub> is increased, but the effect is  
3 smaller than in the original model due to the inclusion of additional chemical reactions. The  
4 behavior is quantitatively consistent with our results except for the highest %O<sub>2</sub> value  
5 (19.5%). As discussed above, it is unclear why the discrepancy for this value.

6

7 *Technical comments 23500, 9, add colon: 'the two absorption band systems of SO<sub>2</sub>:*  
8 *photolysis..andphotoexcitation..'*

9

10 Changed

11

12 *23504, 11, better to write 'transmittance at wavelengths*  
13 *longer than 190 nm'. It is not clear if 'above' refers to energy, wavelength,*  
14 *wavenumber, frequency, etc.*

15

16 Changed

17

18 *23505, 24, I don't see the need for introducing the nonstandard*  
19 *abbreviation 'DCM' for dichloromethane (by the way, the abbreviation is de-*  
20 *fined twice in the text). It is used so few times, only on pages 4 and 5, so that if you*  
21 *really must shorten it, why not write CH<sub>2</sub>Cl<sub>2</sub>?*

22

23 Changed to dichloromethane

24

25 *23509, 19, it is too strict to write '=0'.*  
26 *There is a range of values that would be considered mass-dependent. Suggest either*

1 'approximately equal' or to give the range.

2

3 Changed to "approximately equal". Exact values are subject to controversy.

4

5 23512, 22, *this sentence does not use a*

6 *parallel construction as the first have is an expectation and the second half a seeming*

7 *statement of face. Should the second part rather be, 'but are not expected to reproduce'?*

8

9 Sentence was removed.

10

11 23514, 20, *there's not a clear dividing line between chemistry and physics, so*

12 *it's not clear what is meant here in making a distinction between photochemistry and*

13 *photophysics. Please rewrite using different terminology.*

14

15 Changed

16

17 23514, 25, *it is not clear what*

18 *is meant by 'overprinting'. See comment above under scientific comments,*

19

20 Changed to clarify what is meant

21

22 23514, 12.

23 23529, 5, *the rate given here does not agree with the range of values given in the*

24 *abstract, please be consistent.*

25

26 Changed from rate to order of magnitude estimate and changed manuscript so that it is

1 consistent throughout.

2

1 **J. Savarino (Referee)**

2 jsavarino@ujf-grenoble.fr

3 Received and published: 17 October 2014

4

5 *This manuscript is a new, important and a convincing piece made by the Ono's group*  
6 *regarding the source and origin of the S-MIF in modern sulfate aerosols. After working*  
7 *on the topic for years, the authors reached an impressive mastering of the SO<sub>2</sub>*  
8 *photolysis experiments and their related MIF effects. The paper is really well written*  
9 *exhaustive covering experimental data, molecular dynamic, kinetic chemistry and*  
10 *atmospheric*  
11 *applications. Thus I highly recommend the publication in ACP. This is probably*  
12 *the most accomplished work on the subject, applicable to the present atmosphere.*  
13 *While not yet in direct link with the Archean atmosphere, it is definitely a significant step*  
14 *toward that direction. The present results will certainly help to constrain the structure*  
15 *and composition of the Archean atmosphere, which is currently our main unknown the*  
16 *completely understand the Archean data. Nevertheless, I still want to emphasize that*  
17 *this study should not be considered as the final answer to the issue and more photolysis*  
18 *experiments will be needed to have a complete picture on the topic.*

19

20 We agree that this study is not the final answer. We hope that this study motivates additional  
21 research into this issue.

22

23 *I have only few*  
24 *minor comments and questions before the paper can be published in acp. Note that*  
25 *molecular dynamic is not my field of expertise and thus I did not critically review this*  
26 *part of the paper and thus unable to judge the quality of the work and the limitation of*

1 the interpretation of the calculations, even if the models used are pretty standard in the  
2 field.

3

4 1/ recently Gautier et al. showed at Golsdschmidt2014 a new set of ice core data.  
5 Reporting the data in a  $^{33}\text{S}$  vs  $^{36}\text{S}$  plot, the slope obtained is more around -1.9  
6 than -4 as claimed by the author. Can the author comment on that? can the slope of  
7 -2 been a mixture of photodissociation and photoexcitation or the result of wavelength  
8 dependency effect?

9

10 Added a paragraph to Section 4.7 addressing the possible causes of the discrepancy in  
11 D36S/D33S and discussing the possibility that photoexcitation might contribute to the isotope  
12 signature.

13

14 2/Is the data obtained from the full spectra of the Xe lamp (positive  $^{33}\text{S}$  negative  
15  $^{36}\text{S}$ ) consistent with XS and spectral flux of the lamp?

16

17 Comparisons of full spectral Xe photolysis data with cross-sections has been performed  
18 previously (Whitehill and Ono 2012, Ono et al. 2013). We added a discussion of the cross  
19 sections in Section 4.8 of the revised manuscript.

20

21 3/ Is there any explanation for the large difference observed between replicated experiments?  
22 Large variations are observed for same experimental conditions.

23

24 Added a section (Section 4.8) which discusses caveats with the experimental studies. We do  
25 not have a satisfactory explanation for the observed differences between replicated  
26 experiments except for experimental uncertainties. We hypothesize that it could be due to  
27 differences in the trace amounts of water vapor within the system affecting the chemistry in

1 the cell.

2

3 *4/ Xe or D<sub>2</sub> are significantly different than the solar spectra. How this can impact the*  
4 *obtained results and comparison with ice core data?*

5

6 Added a section (Section 4.8 in revisedmanuscript)where we discuss differences between Xe  
7 and D<sub>2</sub> spectra and the solar spectrum.

8

9 *5/ Why quenching of O1D is assumed to be instantaneous? Quenching is known for*  
10 *O<sub>2</sub> and N<sub>2</sub> and should have been easy to implement in the model or to check the*  
11 *validity of the assumption*

12

13 The model is modified to explicitly model include O(<sup>1</sup>D) chemistry, as well as additional  
14 reactions.

15

16 *6/ is it possible than the high barrier encountered for the TS4 on the singlet PES be*  
17 *lowered by heterogeneous chemistry? can this be explored by the molecular dynamic*  
18 *calculation?*

19

20 Heterogeneous chemistry could be important but is beyond the scope of the present paper.

21

22 *7/ Why the authors have not used the TUV model for the calculation of photolysis rates*  
23 *in the atmosphere (<http://cprm.acd.ucar.edu/Models/TUV/>)? This model has became a*  
24 *standard tool in atmospheric photochemistry*

25

26 Calculations were performed in a very simplified manner using a simple radiative transfer

1 model. The purpose of the model is a first-order estimate of the importance of the proposed  
2 reaction. It is our hope that future modeling studies can

3

4 *8/ Wording about the SO<sub>2</sub> self-limiting effect is ambiguous as it is always the case for*  
5 *any absorbing molecules which by essence limit the radiation for further absorption by*  
6 *the same molecule. I guess they want to say here that taking into account the high*  
7 *concentration of SO<sub>2</sub>, self-shielding can dominate over shielding by other molecules*  
8 *(eg O<sub>3</sub>)*

9

10 It is correct that a self-limiting effect due to shielding is important for all molecules.  
11 However, the isotope effect also depends strongly on shielding by SO<sub>2</sub> (and possibly other  
12 molecules), as demonstrated by Ono et al. (2013). More modeling is necessary to determine  
13 the effect of shielding by ozone and O<sub>2</sub> on the SO<sub>2</sub> absorption in this region.

14

15 *9/ I'm not convinced that self-shielding will decrease the significance of R6 with respect*  
16 *to OH oxidation pathway as OH will also be impacted by the shielding effect but most*  
17 *importantly by the buffering effect (i.e. titration of OH by SO<sub>2</sub>)*

18

19 SO<sub>2</sub> oxidation by OH is catalytic, i.e. it does not consume HO<sub>x</sub>. Models vary as to the  
20 significance of SO<sub>2</sub> loading on HO<sub>x</sub> and OH chemistry. It will also depend upon a number of  
21 other factors, such as the vertical profile of SO<sub>2</sub> and HO<sub>x</sub> species. Such modeling is beyond  
22 the scope of the present paper.

23

24 *10/ The author should add a table displaying the instantaneous fractionation factors.*  
25 *This fundamental for future atmospheric modeling and easy to extract.*

26

27 Exact fractionation factors will vary with temperature and SO<sub>2</sub> column density, as well as

1 other atmospheric conditions (i.e. ozone concentrations, altitude, etc.). For this reason, exact  
2 fractionation factors are not given and should be derived from more advanced modeling  
3 studies. Attempts to provide instantaneous fractionation factors without knowing the exact  
4 position in the atmosphere and atmospheric conditions would be misleading.

5

6 minor remarks

7 *SO<sub>2</sub> and even more O or SO are pretty aggressive compounds. Was there thermocouples*  
8 *protected from oxidation? Can they have reacted with the sulfur compounds?*

9

10 Thermocouples were only used to calibrate the cell with pure N<sub>2</sub>. We assumed the calibration  
11 with pure N<sub>2</sub> is similar to the calibration with a small amount of added SO<sub>2</sub>. This is discussed  
12 in Section 2.1.

13

14 *Why the setup for photodissociation and phototexcitation are different, in particular the*  
15 *SO<sub>2</sub> partial pressure (0.1 kPa vs 1 kPa) or quartz window vs a water IR filter, making*  
16 *the comparison between experiments more difficult.*

17

18 The setup for different experiments are different to maximize product formation and minimize  
19 the effect of the light source on the internal temperature of the cell. The D<sub>2</sub> lamp has a higher  
20 flux in the 190 – 220 nm region (where SO<sub>2</sub> photolysis occurs) and not much infrared  
21 radiation. For SO<sub>2</sub>photoexcitation, a Xe lamp is used due to the higher flux at longer  
22 wavelengths. Because the Xe lamp has a high infrared radiation flux, a water filter was used  
23 to absorb the infrared radiation and prevent it from heating the cell. The water filter was not  
24 used for photolysis experiments because the windows of the cell absorb significantly below  
25 220 nm. Different SO<sub>2</sub> partial pressures are used due to the different cross-section amplitudes  
26 of the two absorption bands. SO<sub>2</sub>photoexcitation is an order of magnitude stronger (i.e.  
27 higher absorption cross-section) than SO<sub>2</sub>photodissociation.

28

29 *Can the spectra of the D2 be given?*

1  
2 The spectral structure of the D<sub>2</sub> lamp is estimated in Whitehill and Ono (2012). The D2 lamp  
3 used here should have a similar spectral structure but a stronger irradiance (due to it being 200  
4 W versus 30 W).

5  
6 *Can the shorter wavelengths open another exit  
7 channel?*

8  
9 The glass used for the cell windows (Corning 7980) absorbs significantly below around 180  
10 nm to 200 nm, preventing chemistry from the higher energy dissociation band (< 165 nm) of  
11 SO<sub>2</sub> from occurring under our experimental conditions. In addition, in experiments  
12 performed in room air (versus a nitrogen atmosphere), air absorbs almost all the radiation  
13 below around 195 nm. This is discussed in Whitehill and Ono (2012).

14  
15 *Do the author have any idea of the humidity present in the cell/flowing gases and thus  
16 have an idea of the lifetime of SO<sub>3</sub> to check if their assumption of collecting 100% of  
17 SO<sub>3</sub> makes sense?*

18  
19 We do not have constraints on the amount of water within the cell. However, the kinetic  
20 model of the cell chemistry is modified to include HO<sub>x</sub> chemistry and an estimate of the  
21 amount of water in the cell is made. Attempts to constrain the amount of SO<sub>3</sub> formation  
22 based purely on the SO<sub>3</sub> + 2H<sub>2</sub>O reaction produce unreasonably small product formation  
23 rates, suggesting additional processes (i.e. heterogeneous processes or wall absorption  
24 processes) must be trapping SO<sub>3</sub> in the system.

25  
26 *Can the authors give the lamp and filters used in caption tables?*  
27  
28 Table 1 summarizes the lamps and filters used in the various experiments for the rest of the

1 tables.

2

3 *Many times eq(5) cited in the text actually corresponds to eq(4).*

4

5 This was an error in the conversion from Word to Latex. This will be corrected in the final  
6 version.

7

8 *Table 4: column 4 yield/umol S, technically this is not a yield but an amount*

9

10 (Absolute) yield is the amount of product obtained in a chemical reaction (in grams or moles),  
11 which is what is reported. Therefore, we believe that yield has been used correctly in this  
12 case.

13

14 *Why in figure 3, the LP experiments show a small MIF when table 3 displays a large  
15 effect for the photoexcitation?*

16

17 In the experiments reported in Table 3, 100% of the product comes from  ${}^3\text{SO}_2$ , so the isotope  
18 signature is not diluted. In the results displayed in Figure 3, most of the  $\text{SO}_3$  likely comes  
19 from the  ${}^3\text{SO}_2 + \text{SO}_2 \rightarrow \text{SO}_3 + \text{SO}$  reaction, which produces mass-dependent  $\text{SO}_3$  (see Whitehill  
20 and Ono 2012). A small amount of the  $\text{SO}_3$  comes from a mass-dependent channel, such as  
21  ${}^3\text{SO}_2 + \text{O}_2 \rightarrow \text{SO}_3 + \text{O}$  (Hattori et al. 2013) or  $\text{SO} + \text{O}_2 + \text{M} \rightarrow \text{SO}_3 + \text{M}$  (with  $\text{SO}$  from  ${}^3\text{SO}_2 +$   
22  $\text{SO}_2$  reaction). Therefore, the product sulfate from the photoexcitation experiments in Figure  
23 3 are diluted by a significant amount of mass-dependent sulfate.

24 |

1 **SO<sub>2</sub> photolysis as a source for sulfur mass-independent**  
2 **isotope signatures in stratospheric aerosols**

3  
4 **A. R. Whitehill<sup>1</sup>, B. Jiang<sup>2</sup>, H. Guo<sup>2</sup>, and S. Ono<sup>1</sup>**  
5 [1]{Department of Earth, Atmospheric, and Planetary Sciences, Massachusetts Institute of  
6 Technology, 77 Massachusetts Ave., Cambridge, MA 02139, USA}  
7 [2]{Department of Chemistry and Chemical Biology, University of New Mexico,  
8 Albuquerque, NM 87131, USA}  
9 Correspondence to: A.R. Whitehill (arwhite@mit.edu)  
10

11 **Abstract**

12 Signatures of sulfur isotope mass-independent fractionation(S-MIF) have been observed in  
13 stratospheric sulfate aerosols deposited in polar ice. The S-MIF signatures are thought to be  
14 associated with stratospheric photochemistry following stratospheric volcanic eruptions, but  
15 the exact mechanism responsible for the production and preservation of these signatures is  
16 debated. In order to identify the origin and the mechanism of preservation for these signatures,  
17 a series of laboratory photochemical experiments were carried out to investigate the effect of  
18 temperature and added O<sub>2</sub> on S-MIF produced by the two absorption band systems of SO<sub>2</sub>:—  
19 photolysis in the 190 nm to 220 nm region and photoexcitation in the 250 nm to 350 nm  
20 region. The SO<sub>2</sub> photolysis (SO<sub>2</sub>+hv→ SO + O) experiments showed S-MIF signals with  
21 large <sup>34</sup>S/<sup>32</sup>S fractionation, which increases with decreasing temperature. The overall S-MIF  
22 pattern observed for photolysis experiments, including high <sup>34</sup>S/<sup>32</sup>S fractionations, positive  
23 mass-independent anomalies in <sup>33</sup>S, and negative anomalies in <sup>36</sup>S, is consistent with a major  
24 contribution from optical isotopologue screening effects and measurements—data for  
25 stratospheric sulfate aerosols. In contrast, SO<sub>2</sub>photoexcitation produced products with  
26 positive MIF anomalies in both <sup>33</sup>S and <sup>36</sup>S that is different from stratospheric aerosols. SO<sub>2</sub>  
27 photolysis in the presence of O<sub>2</sub>produced SO<sub>3</sub> with S-MIF signals, suggesting the transfer of  
28 the MIF signals of SO to SO<sub>3</sub> by the SO + O<sub>2</sub> + M → SO<sub>3</sub> + M reaction. This is supported  
29 with energy calculations of stationary points on the SO<sub>3</sub> potential energy surfaces,

1 which indicate that this reaction occurs slowly on a single adiabatic surface, but that it can  
2 occur more rapidly through intersystem crossing. Based on our experimental results, we  
3 estimate a termolecular rate constant on the order of  $10^{-37} \text{ cm}^6 \text{ molecule}^{-2} \text{ s}^{-1}$ . The results from  
4 our experiments constrain the termolecular reaction rate to between  $1.0 \times 10^{-37} \text{ cm}^6 \text{ molecule}^{-2}$   
5  $\text{s}^+$  and  $1.0 \times 10^{-36} \text{ cm}^6 \text{ molecule}^{-2} \text{ s}^+$ . This rate can explain the preservation of mass  
6 independent isotope signatures in stratospheric sulfate aerosols and provides a minor, but  
7 important, oxidation pathway for stratospheric  $\text{SO}_2$ . above about 25 km altitude. The  
8 production and preservation of S-MIF signals in the stratosphere requires a high  $\text{SO}_2$  column  
9 density to allow for optical isotopologue screening effects to occur and to generate a large  
10 enough signature that it can be preserved. In addition, the ~~and~~  $\text{SO}_2$  plume must reach an  
11 altitude of around 20 to 25 km, where  $\text{SO}_2$  photolysis becomes a dominant process reaching an  
12 altitude of 25 km and higher. These experiments are the first step towards understanding the  
13 origin of the sulfur isotope anomalies in stratospheric sulfate aerosols.

Formatted: Subscript

14

15 **1 Introduction**

16 Explosive volcanic eruptions that inject sulfur dioxide ( $\text{SO}_2$ ) into the stratosphere can  
17 cause perturbations to the stratospheric sulfur cycle for years following eruptions. The  
18 increase in stratospheric sulfate aerosols associated with injections of  $\text{SO}_2$  result in  
19 stratospheric warming and tropospheric cooling, and can also trigger changes in atmospheric  
20 circulation and increases in ozone depletion (Robock, 2000). Perturbations to the stratospheric  
21 sulfur cycle following large volcanic eruptions are recorded as changes in sulfur isotope  
22 ratios, as measured in stratospheric sulfate aerosol samples (Castleman et al., 1974), as well as  
23 in ice core records (Savarino et al., 2003; Baroni et al., 2007).

Formatted: Indent: First line: 0.3"

24 The reaction with OH is the dominant oxidation pathway for  $\text{SO}_2$  in the stratosphere:



26 This reaction is followed by:



28 In the presence of  $\text{H}_2\text{O}$ ,  $\text{SO}_3$  readily forms sulfuric acid ( $\text{H}_2\text{SO}_4$ ) via:



1 Ab-initio transition state theory calculations of the isotope effect for OH oxidation (R1) - - - Formatted: Indent: First line: 0.49"  
2 predict that  $^{34}\text{SO}_2$  is oxidized 0.9% slower than  $^{32}\text{SO}_2$  (Tanaka et al., 1994), although  
3 calculations with RRKM theory predicts an inverse isotope effect, in which  $^{34}\text{SO}_2$  reacts 12%  
4 to 15% faster than  $^{32}\text{SO}_2$  (Leung et al., 2001). Experimental studies of OH oxidation  
5 (R1) showed in an inverse isotope effect, but with a smaller magnitude, with  $^{34}\text{SO}_2$  reacting  
6 about 1% faster than  $^{32}\text{SO}_2$  (Harris et al., 2012). Although the~~the~~ The experimentally measured  
7 isotope effect ~~is in~~~~not~~ might be sufficient to explain the roughly 2% enrichment in  $\text{H}_2^{34}\text{SO}_4$   
8 relative to  $\text{H}_2^{32}\text{SO}_4$  following the major Mt. Agung (1963) eruption (Castleman et al., 1974).  
9 the large observed isotope effect suggests the possibility of an additional oxidation reaction  
10 with larger  $^{34}\text{S}$  fractionations.

11 ~~An additional oxidation reaction is necessary to explain the sulfur isotope effects in~~  
12 ~~stratospheric sulfate aerosols following large volcanic eruptions.~~

13 An additional unexplained observation is the isotope anomalies in  $^{33}\text{S}/^{32}\text{S}$  and  $^{36}\text{S}/^{32}\text{S}$  ratios  
14 relative to  $^{34}\text{S}/^{32}\text{S}$  ratios. These signatures of mass-independent fractionation (MIF) have been  
15 observed in ice cores associated with large volcanic eruptions (Savarino et al., 2003; Baroni et  
16 al., 2007, 2008; Lanciki, 2010; Lanciki et al., 2012). Ice core sulfate peaks are commonly  
17 used to reconstruct the impact of past volcanic activity, which is critical to forcing climate  
18 models (Robock, 2000). For several years following large injections of  $\text{SO}_2$  into the  
19 stratosphere, stratosphere-derived sulfate can dominate sulfate deposition in ice cores and,  
20 ~~when~~~~if~~ corrected for background levels, can preserve the sulfur isotopic composition of  
21 stratospheric sulfate aerosols. Experimental studies demonstrate that OH oxidation of  $\text{SO}_2$   
22 (R1) does not produce mass-independent sulfur isotope anomalies (Harris et al., 2012, 2013),  
23 so an additional oxidation mechanism is required to produce the mass-independent sulfur  
24 isotope signatures. Three reactions have been proposed to explain these isotope anomalies:  
25 excited-state photochemistry of  $\text{SO}_2$  in the 250 nm to 350 nm absorption region (Savarino et  
26 al., 2003; Hattori et al., 2013),  $\text{SO}_2$  photolysis in the 190 nm to 220 nm absorption region  
27 (Ono et al., 2013), and  $\text{SO}_3$  photolysis (Pavlov et al., 2005).

28 We present results of laboratory photochemical experiments that support  $\text{SO}_2$  - - - Formatted: Indent: First line: 0.49"  
29 photolysis as the main source for the MIF signatures observed in stratospheric sulfate aerosols  
30 following some large (stratospheric) volcanic eruptions. In particular,  $\text{SO}_2$  photolysis  
31 produces large MIF anomalies, as well as large mass-dependent isotope fractionations  
32 (Masterson et al., 2011; Whitehill and Ono, 2012; Ono et al., 2013) that are consistent with

1 the isotopic signatures observed in stratospheric sulfate aerosols in ice cores (Ono et al.,  
2 ~~Even a minor contribution of SO<sub>2</sub> photolysis to the production of sulfate aerosols can~~  
3 ~~have a major influence on the isotope ratios of sulfur.~~

4 Photolysis of SO<sub>2</sub> occurs above around 20 to 25 km in the wavelength region of 190  
5 nm to 220 nm, which lies in the spectral window between the Schumann-Runge absorption  
6 edge of oxygen (O<sub>2</sub>) and the Hartley bands of ozone (O<sub>3</sub>). SO<sub>2</sub> photolysis produces sulfur  
7 monoxide (SO) and O(<sup>3</sup>P) via the following reaction:



9 It is generally accepted that this reaction is followed by rapid oxidation of SO to SO<sub>2</sub>  
10 via (Black et al., 1982; Savarino et al., 2003; Pavlov et al., 2005):



12 Reactions R4 and R5 combine to form a null cycle for sulfur, but catalyze the formation of  
13 odd oxygen (Bekki, 1995). If SO is completely oxidized to SO<sub>2</sub>, no isotopic signature from  
14 SO<sub>2</sub> photolysis can be preserved (Pavlov et al., 2005).

15 We propose an additional channel where SO is oxidized directly to SO<sub>3</sub> via the  
16 termolecular reaction:



18 A previous study by Black et al. (1982) showed that the maximum termolecular rate constant  
19 for reaction R6 is  $10^{-36}$  cm<sup>6</sup> molecule<sup>-2</sup> s<sup>-1</sup>. This rate is considered too slow to play an  
20 important role for stratospheric chemistry (Black et al., 1982). However, given the large  
21 isotope effects produced during SO<sub>2</sub> photolysis, even a minor contribution from R6 will  
22 produce a significant signal on the sulfur isotopic composition of stratospheric sulfate  
23 aerosols.

24 We present results from laboratory photochemical experiments that investigate the effect  
25 of temperature and molecular oxygen on the isotope effects produced during SO<sub>2</sub> photolysis  
26 (190 nm to 220 nm) and SO<sub>2</sub> photoexcitation (250 nm to 350 nm). Using the results of the  
27 experiments in the presence of molecular oxygen, we calculate a lower bound estimate on the  
28 rate of R6. In addition, our proposal is further supported by ab-initio calculations of  
29 stationary points along the potential energy surfaces (PESs) for the SO oxidation reactions  
30 (R5 and R6). Finally, we present a simple steady state photochemical model to show that the

Formatted: Indent: First line: 0.49"

Formatted: Indent: First line: 0.49"

Formatted: Indent: First line: 0.3"

1 rate constraints on reaction R6 are sufficient for it to make a significant contribution to the  
2 isotopic signature of stratospheric sulfate aerosols during volcanically perturbed periods.

3 **2 Methods**

4 **2.1 Photochemical reaction set-up**

5 Conditions for all photochemical experiments are listed in Table 1. All experiments were  
6 performed in a cylindrical glass photochemical reaction cell with a pathlength of 15.3 cm and  
7 an inner diameter of 5.2 cm (Ono et al., 2013). Temperature-controlled experiments were  
8 performed in a jacketed cell of the same dimensions. The front window of the cell was made  
9 of UV-grade SiO<sub>2</sub> (Corning 7980) with greater than 90% transmittance above at wavelengths  
10 longer than 190 nm. The window was sealed to the cell with an o-ring and held in place  
11 securely with a plastic clamp. Temperature-controlled experiments also utilized a second pre-  
12 cell (5.3 cm pathlength) attached to the front window of the reaction cell and held under  
13 vacuum. The purpose of the pre-cell was to thermally insulate the front window and prevent  
14 condensation from occurring on the front window during low temperature experiments.

15 A series of mass-flow controllers controlled the flow rate of gases into the cell. Gas entered  
16 the cell through an inlet at the rear of the cell (for temperature cell experiments) or the front of  
17 the cell (for other experiments) and exited the cell through an outlet at the opposite end of the  
18 cell. An 8 cm to 10 cm length of glass tubing packed with glass wool was placed  
19 immediately after the cell exit to trap aerosols formed within the cell. Following the aerosol  
20 trap, the gas was flowed through a proportionating valve to a vacuum pump. A capacitance  
21 manometer placed before the entrance to the cell monitored the pressure within the cell. The  
22 proportionating valve was used to control the pressure within the cell to within 30 Pa of a  
23 setpoint pressure, which was usually 101.3 kPa.

24 Prior to each temperature-controlled experiment, the reaction cell was flushed with  
25 nitrogen(N<sub>2</sub>) for several hours and the chiller was allowed to reach its setpoint temperature  
26 and equilibrate for at least an hour. The temperature of the reaction cell was calibrated  
27 relative to the chiller setpoint temperature on two occasions using a series of K-type  
28 thermocouples suspended within the cell. During calibrations, N<sub>2</sub>(without SO<sub>2</sub>) was flowed  
29 through the cell at a rate of 3.33 cm<sup>3</sup> s<sup>-1</sup> (200 sccm, standard cubic centimeter per minute).  
30 Thermocouples placed at the front and rear of the cell gave consistent measurements to within

Formatted: Subscript

1 5 K, with a higher gradient at lower temperatures. No significant differences were observed  
2 between the two calibrations. Results for the temperature calibration are shown in Figure 1.

3 **2.2 Temperature effect on SO<sub>2</sub> photolysis (190 nm to 220 nm) and**  
4 **photoexcitation (250 nm to 350 nm)**

5 The temperature effect on SO<sub>2</sub> photolysis (190 nm to 220 nm) was ~~measured tested~~ using the  
6 temperature-controlled reaction cell described in Section 2.1. Experiments were performed in  
7 a nitrogen-flushed glove box to prevent the spectral interference from the Schumann-Runge  
8 band of oxygen (O<sub>2</sub>). A 200 W deuterium (D<sub>2</sub>) arc lamp (D 200 F, HeraeusNoblelight) was  
9 used as the light source without optical filters. The output from the lamp was collimated  
10 using a fused silica plano-convex lens. 1000 ppm SO<sub>2</sub> (in N<sub>2</sub>) was flowed through the cell at  
11 a rate of 3.33 cm<sup>3</sup> s<sup>-1</sup> (200 sccm) for all experiments, and pressure within the cell was held  
12 constant at 101.3 kPa, giving an SO<sub>2</sub> partial pressure of 0.10 kPa within the cell.

13 Following photolysis experiments, the cell was removed from the glove box and rinsed well  
14 with dichloromethane (~~DCM~~) to dissolve any elemental sulfur that was formed. The glass  
15 wool in the aerosol trap was also collected and rinsed with ~~DCM~~dichloromethane. Elemental  
16 sulfur was recrystallized from ~~DCM-dichloromethane~~ and converted to silver sulfide using the  
17 reduced chromium chloride method (Whitehill and Ono, 2012; Canfield et al., 1986).  
18 Multiple sulfur isotope ratios were measured as described in Section 2.4.

19 Photoexcitation experiments were performed in a room air atmosphere using a 150 W UV-  
20 enhanced xenon (Xe) arc lamp (Newport Model 6254) housed in a lamp housing (Newport  
21 Model 67005), which focused and collimated the light to a 3.3 cm diameter beam. The light  
22 was passed through a liquid filter (Newport Model 51945) filled with deionized (18.2 MΩ)  
23 water and a 250 nm longpass filter (Asahi Spectra, ZUL0250).

24 Following Whitehill et al. (2013), acetylene (C<sub>2</sub>H<sub>2</sub>) was used to trap triplet excited-state SO<sub>2</sub>  
25 (<sup>3</sup>SO<sub>2</sub>). During experiments, 5% SO<sub>2</sub> (in N<sub>2</sub>), pure C<sub>2</sub>H<sub>2</sub> (Atomic Absorption Grade), and  
26 pure N<sub>2</sub> (Ultra High Purity grade) were flowed through the cell continuously at a rate of 0.67  
27 cm<sup>3</sup> s<sup>-1</sup> (40 sccm), 0.03 cm<sup>3</sup> s<sup>-1</sup> (2 sccm), and 2.63 cm<sup>3</sup> s<sup>-1</sup> (158 sccm), respectively. Pressure  
28 in the cell was held constant at 101.3 kPa, giving a total flow rate of 3.33 cm<sup>3</sup> s<sup>-1</sup>, an SO<sub>2</sub>  
29 partial pressure of 1.01 kPa, and a C<sub>2</sub>H<sub>2</sub> partial pressure of 1.01 kPa within the cell during the  
30 experiments.

1 Following the experiments, the interior walls of the cell and the window were rinsed with  
2 ethanol and water to dissolve any organosulfur products formed. The glass wool in the  
3 aerosol trap was also collected. The organosulfur aerosol products were converted to silver  
4 sulfide using the Raney nickel hydrodesulfurization method of Oduro et al. (2011). Multiple  
5 sulfur isotope ratios were measured as described in Section 2.4.

### 6 **2.3 SO<sub>2</sub> photochemistry in the presence of O<sub>2</sub>**

7 The photochemistry of SO<sub>2</sub> + O<sub>2</sub> with ultraviolet radiation was studied using a reaction cell at  
8 room temperature. The 150 W Xe arc lamp (described in Section 2.2) was used as the light  
9 source without the liquid filter. Several experiments were performed with a 200 ± 35 nm  
10 bandpass filter (Model 200-B, Acton Research, Acton, MA), a 250 nm longpass filter (Asahi  
11 Spectra, ZUL0250), or a 280 nm (285 nm cut-on)longpass filter (Newport Model FSR-  
12 WG280) to isolate particular absorption bands of SO<sub>2</sub>, but most experiments were performed  
13 with the Xe lamp and no filters ([Table 1](#)).

14 Following experiments, the cell was rinsed well first with dichloromethane (~~DCM~~) then with  
15 water. Although sulfate was the dominant product, the cell was rinsed well with  
16 dichloromethane-DCM first to ensure the removal of elemental sulfur. For two experiments  
17 performed with no oxygen, elemental sulfur was recovered. After rinsing the cell with water,  
18 5.0 cm<sup>3</sup> of a 1.0 mol dm<sup>-3</sup> solution of barium chloride (BaCl<sub>2</sub>) was added to the water used to  
19 rinse the cell to precipitate sulfate as barium sulfate. Barium sulfate was rinsed several times  
20 with deionized water and dried. The glass wool inside the aerosol trap was combined with the  
21 barium sulfate and all sulfate was converted to silver sulfide using the method of Forrest and  
22 Newman (1977). Multiple sulfur isotope ratios were measured as described in Section 2.4.

### 23 **2.4 Isotope analysis of photochemical products**

24 Photochemical products were converted to silver sulfide (Ag<sub>2</sub>S). Ag<sub>2</sub>S was rinsed well three  
25 to four times with deionized water and then dried completely at 353 K. Dried Ag<sub>2</sub>S was  
26 weighed for total yield and about 8 µmol of Ag<sub>2</sub>S was weighed into an aluminum foil capsule  
27 for isotope analysis. Capsules were loaded into nickel reaction chambers and reacted under  
28 approximately 7.3 kPa of fluorine gas (F<sub>2</sub>) for at least 8 hours at 573 K. The resultant SF<sub>6</sub>  
29 was purified cryogenically and by gas chromatography. Isotope ratios of pure SF<sub>6</sub> were  
30 measured as SF<sub>5</sub><sup>+</sup> ions using a Thermo Scientific MAT 253 Isotope Ratio Mass Spectrometer.

1 For samples where less than 1.6 $\mu$ mol of Ag<sub>2</sub>S was recovered, a microvolume (0.4 cm<sup>3</sup>  
2 volume) coldfinger was used to concentrate the samples for analysis.

3 Replicate analyses ( $N = 28$ ) of the reference material IAEA-S-1 gave  $2\sigma$  standard  
4 deviations of 0.26 ‰ for  $\delta^{34}\text{S}$ , 0.014 ‰ for  $\Delta^{33}\text{S}$ , and 0.19 ‰ for  $\Delta^{36}\text{S}$  for standard isotope  
5 ratio mass spectrometry analysis. Microvolume analyses for smaller samples gave  $2\sigma$   
6 standard deviations for replicate analyses of IAEA-S-1 ( $N = 14$ ) of 0.9 ‰ for  $\delta^{34}\text{S}$ , 0.08 ‰ for  
7  $\Delta^{33}\text{S}$ , and 0.8 ‰ for  $\Delta^{36}\text{S}$ . Replicate experiments performed under identical conditions had  
8 differences larger than the analytical uncertainty, suggesting experimental variability was the  
9 dominant source of uncertainty in our measurements.

## 10 2.5 Potential energy surfaces of SO + O<sub>2</sub> → SO<sub>3</sub> → SO<sub>2</sub> + O reactions

11 To test the feasibility of reaction R6, ab-initio energy calculations at multiple levels of theory  
12 were performed to search important stationary points on the SO<sub>3</sub>potential energy surfaces  
13 (PESs). The lowest SO(<sup>3</sup> $\Sigma^-$ ) + O<sub>2</sub>(<sup>3</sup> $\Sigma_g^-$ ) asymptote of the SO<sub>3</sub> PESs involves three degenerate  
14 states, namely the singlet, triplet, and quintet states. The singlet state corresponds to the  
15 ground state of the SO<sub>3</sub> molecule (<sup>1</sup>A<sub>1</sub>), but does not dissociate to the ground state products  
16 SO<sub>2</sub>(<sup>1</sup>A<sub>1</sub>) + O(<sup>3</sup>P) but to SO<sub>2</sub>(<sup>1</sup>A<sub>1</sub>) + O(<sup>1</sup>D). The triplet surface corresponds to the ground  
17 state products but is adiabatically associated with a higher energy excited-state (triplet) SO<sub>3</sub>.  
18 The quintet state is much higher in energy than the other two states except at the SO(<sup>3</sup> $\Sigma^-$ ) +  
19 O<sub>2</sub>(<sup>3</sup> $\Sigma_g^-$ ) asymptote and will thus not be considered in this study.

20 The B3LYP density functional (Becke, 1988; Lee et al., 1988) was initially used to optimize  
21 each minimum and/or transition state on the singlet and triplet potential energy surfaces  
22 Single point calculations at these stationary points were then carried out using an explicitly  
23 correlated version of the unrestricted coupled cluster method with single, double and  
24 perturbative triple excitations method (UCCSD(T)-F12a; Knizia et al., 2009).

25 In addition, complete active space self-self-consistent field (CASSCF) calculations were  
26 performed (Knowles and Werner, 1985, 1988). Multi-reference Rayleigh Schrödinger  
27 perturbation theory of second order (RSPT2 or CASPT2) calculations (Celani and Werner,  
28 2000) were performed based on the CASSCF wavefunctions in order to account for part of  
29 the dynamical correlation. Calculations including the full valence orbitals would involve 24  
30 electrons in 16 orbitals and were not feasible. Instead, the 2s orbital for O and the 3s orbital  
31 for S were closed, resulting in an active space of 16 electrons in 12 orbitals (16e,12o).

1 Dunning's augmented correlation-consistent polarized valence triplet-zeta (aug-cc-pVTZ)  
2 basis set was used in all cases (Dunning, 1989). B3LYP calculations were performed with  
3 Gaussian09 (Frisch et al., 2009) and the other calculations were performed using  
4 MOLPRO(Werner et al., 2012).

5 **2.6 Definitions**

6 Isotopic results will be presented with conventional  $\delta$  notation, as relative deviations of  
7 isotope ratios with respect to reference sulfur.

8 
$$\delta^x S = \frac{x R_{product}}{x R_{reference}} - 1 \quad (1)$$

9 where  $x = 33, 34$ , or  $36$  and  $x R$  is the ratio of  $^x S$  to  $^{32} S$  in the substance. For experimental  
10 results all isotope ratios will be normalized to the isotope ratios of the initial  $SO_2$ . For natural  
11 samples (i.e. stratospheric sulfate aerosol samples), the reference is Vienna Canyon Diablo  
12 Troilite (V-CDT).

13 Mass-independent isotope fractionations in  $^{33} S/^{32} S$  and  $^{36} S/^{32} S$  ratios (relative to  $^{34} S/^{32} S$  ratios)  
14 will be presented as  $\Delta^{33} S$  and  $\Delta^{36} S$  values, respectively. These are defined as:

15 
$$\Delta^{33} S = \frac{(\delta^{33} S + 1)}{(\delta^{34} S + 1)^{0.515}} - 1 \quad (2)$$

16 and

17 
$$\Delta^{36} S = \frac{(\delta^{36} S + 1)}{(\delta^{34} S + 1)^{1.90}} - 1 \quad (3)$$

18 Almost all physical, chemical, and biological processes fractionate isotopes mass-dependently  
19 (i.e.  $\Delta^{33} S$  and  $\Delta^{36} S$  are approximately equal to = 00 and  $\Delta^{36} S = 0$ ).  $SO_2$ photochemistry, as  
20 well as the photochemistry of other sulfur gases such as  $CS_2$ , are some of the few exceptions  
21 that have been shown to produce mass-independent fractionation. Therefore, non-zero  $\Delta^{33} S$   
22 and  $\Delta^{36} S$  values can be unique tracers of photochemical processes.

23 **3 Results**

24 All experiments performed are summarized in Table 1. Results from temperature  
25 experiments on  $SO_2$  photolysis and  $SO_2$ photoexcitation are given in Tables 2 and 3, whereas

1 results from  $\text{SO}_2 + \text{O}_2$  experiments are presented in Tables 4 and 5. Tables 6, 7, and 8 give  
2 the results from energy calculations on the [potential energy surfaces PESs](#) of  $\text{SO}_3$ .

3 **3.1 Temperature experiments**

4 Results from the temperature experiments (Section 2.2) are shown in Figure 2. The  $\text{SO}_2$   
5 photolysis (190 nm to 220 nm) experiments (Table 2) revealed that the magnitude of the  
6 isotope effects increase with decreasing temperatures, from 129‰ to 191‰, 5.5‰ to 9.1‰  
7 and -24.1‰ to -35.8‰, for  $\delta^{34}\text{S}$ ,  $\Delta^{33}\text{S}$ , and  $\Delta^{36}\text{S}$ , respectively. The relationship between  
8 isotopes (i.e.  $\Delta^{33}\text{S}$  versus  $\delta^{34}\text{S}$  and  $\Delta^{36}\text{S}$  versus  $\Delta^{33}\text{S}$ ) did not change significantly as  
9 temperature was decreased (0.04 to 0.05 for  $\Delta^{33}\text{S}/\delta^{34}\text{S}$  and -3.9 to -4.6 for  $\Delta^{36}\text{S}/\Delta^{33}\text{S}$ ).

10 Variability between duplicate experiments also increased at lower temperatures, highlighting  
11 the difficulty of the low temperature experiments and indicating a strong sensitivity to  
12 experimental conditions.

13  $\text{SO}_2$  photoexcitation (250 nm to 350 nm) showdecreasing magnitude  $\Delta^{33}\text{S}$  and  $\Delta^{36}\text{S}$  values at  
14 lower temperatures (22.8‰ to 19.0‰ and 52.5‰ to 46.0‰ for  $\Delta^{33}\text{S}$  and  $\Delta^{36}\text{S}$ , respectively;  
15 Table 3). Even at lower temperatures, the product from  $\text{SO}_2$  photoexcitation experiments  
16 show positive  $\Delta^{33}\text{S}$  and  $\Delta^{36}\text{S}$  values, as shown previously in room-temperature experiments  
17 (Whitehill and Ono, 2012; Whitehill et al., 2013). As discussed previously (Whitehill et al.,  
18 2013), these signatures do not match predictions from isotopologue-specific absorption cross-  
19 sections (Danielache et al., 2012), suggesting an additional isotope effect beyond differences  
20 in the initial excitation for different isotopologues.

21 **3.2 Oxygen experiments**

22  $\text{SO}_2$  photolysis and photoexcitation in the presence of molecular oxygen ( $\text{O}_2$ ) produced mass-  
23 independent sulfur isotope signatures in sulfate products (Tables 4 and 5). Isotope ratios of  
24 this product sulfate are shown in Figure 3 and compared with stratospheric sulfate aerosol  
25 data from ice cores (Savarino et al., 2003; Baroni et al., 2007, 2008; Lanciki, 2010; Lanciki et  
26 al., 2012). Strong agreement between the Xe lamp data, 200 nm bandpass (200 BP) data, and  
27 previous  $\text{SO}_2$  photolysis data (Ono et al., 2013) suggest an  $\text{SO}_2$  photolysis source for the  
28 isotope effects during broadband  $\text{SO}_2$  irradiation with the Xe lamp light source.

29 Experiments focusing on the photoexcitation band of  $\text{SO}_2$  using the 250 nm longpass filter  
30 (250 LP) and 280 nm longpass filter (280 LP) display a different isotope signature,

1 characterized by positive  $\Delta^{33}\text{S}$  and  $\Delta^{36}\text{S}$  values, whereas sulfate from  $\text{SO}_2$  photolysis has  
2 positive  $\Delta^{33}\text{S}$  and negative  $\Delta^{36}\text{S}$  values. This is consistent with previous findings (Whitehill  
3 and Ono, 2012; Whitehill et al., 2013), and demonstrates the MIF in this band region is not  
4 produced by chemistry related to acetylene nor oxygen. However, the magnitude of the sulfur  
5 MIF signatures (i.e.  $\Delta^{33}\text{S}$  and  $\Delta^{36}\text{S}$  values) are considerably smaller than previous experiments  
6 using  $\text{C}_2\text{H}_2$  (Table 3, Whitehill et al., 2013). This suggests that a considerable amount of the  
7 sulfate in the system is being produced by a mass-dependent process, such as  $^*\text{SO}_2 + \text{SO}_2 \rightarrow$   
8  $\text{SO} + \text{SO}_3$  (Whitehill and Ono, 2012). This would dilute the MIF signature. In addition, there  
9 is considerable variability (i.e. a factor of ~2) was observed between the two 250 nm longpass  
10 filter experiments, despite identical experimental conditions. The cause of this variability is  
11 uncertain but could relate to the amount of water vapor within the system.

### 12 3.3 Potential energy surfaces of $\text{SO}_3$

13 Asymptotic energies of  $\text{SO} + \text{O}_2$  on each potential energy surfacePES were compared with the  
14 energies obtained by separate calculations of each species with a certain spin (Table 6). The  
15 CASSCF results correctly produced degenerate energies for the  $\text{SO} + \text{O}_2$  asymptote on the  
16 singlet and triplet states, which exactly match the sum of the energies of ~~the~~ the  $\text{SO}({}^3\Sigma^-)$  and  
17  $\text{O}_2({}^3\Sigma_g^-)$ species calculated separately. The CASPT2 results also showed the correct degenerate  
18 behavior but the energies shift slightly from those calculated separately, which presumably  
19 arises from the perturbative treatment in CASPT2~~on~~. On the other hand, the UCCSD(T)-F12a  
20 and B3LYP results both attribute  $\text{SO} + \text{O}_2$  on the singlet state to  $\text{SO}({}^1\Delta) + \text{O}_2({}^1\Delta_g)$ , and B3LYP  
21 even gives a qualitatively incorrect energy for  $\text{SO} + \text{O}_2$  on the triplet state, while UCCSD(T)-  
22 F12a attributes the triplet state this one to  $\text{SO}({}^1\Delta) + \text{O}_2({}^3\Sigma_g^-)$ . An important conclusion from  
23 these data is that one has to use a multi-reference method if ~~an~~ accurate global adiabatic  
24 potential energy surfacePES~~is~~ are desired for this system. Otherwise, the asymptotic behavior  
25 can be completely wrong. None of the previous studies has noticed this, and as a result a  
26 single-reference method was always selected (Jou et al., 1996; Martin, 1999; Goodarzi et al.,  
27 2010; Ahmed, 2013). Fortunately, single reference methods can accurately describe the PES  
28 away from the  $\text{SO} + \text{O}_2$  region; they are capable of describing several  $\text{SO}_3$  isomers and the  
29  $\text{SO}_2 + \text{O}$  product channel reasonably well.

30 Energies for the stationary points computed using multi-reference approaches are reported  
31 relative to that of the  $\text{SO}({}^3\Sigma^-) + \text{O}_2({}^3\Sigma_g^-)$  asymptote. However, the active space used in our  
32 CASSCF calculations is not sufficient to provide quantitatively accurate results, but a larger

Formatted: Justified

1 active space is still computationally infeasible. For single-reference calculations, we chose to  
2 use the UCCSD(T) energies at optimized B3LYP geometries for the stationary points. To  
3 avoid the aforementioned problems in the  $\text{SO}(^3\Sigma^-) + \text{O}_2(^3\Sigma_g^-)$  asymptote, we have used the  
4 UCCSD(T) energy sum of the two reactants with the correct spins calculated separately, which  
5 has been shown [above](#) to be accurate. The sum of these two energies thus provides the  
6 reference for other stationary points on both singlet and triplet PESs. All energies of  
7 stationary points are listed in Tables 7 and 8, and the reaction pathways on both PESs are  
8 shown graphically in Figure 4, using the energies of the UCCSD(T)//B3LYP calculations. It is  
9 seen from Tables 7 and 8 that the experimental derived energy differences (from Chase, 1986)  
10 between reactants and products for the  $\text{SO}(^3\Sigma^-) + \text{O}_2(^3\Sigma_g^-) \rightarrow \text{SO}_3(^1A_1')$  reaction (-411.29 kJ  
11 mole<sup>-1</sup>), the  $\text{SO}(^3\Sigma^-) + \text{O}_2(^3\Sigma_g^-) \rightarrow \text{SO}_2(^1A_1) + \text{O}(^3P)$  reaction (-54.56 kJ mole<sup>-1</sup>) and the  $\text{SO}(^3\Sigma^-)$   
12  $+ \text{O}_2(^3\Sigma_g^-) \rightarrow \text{SO}_2(^1A_1) + \text{O}(^1D)$  reaction (135.27 kJ mole<sup>-1</sup>) are reproduced well by the  
13 UCCSD(T)-F12a//B3LYP calculations, while the other methods contain significant errors.

## 14 4 Discussion

### 15 4.1 Origin of mass-independent fractionation during $\text{SO}_2$ photochemistry

16 ~~Isotopologue specific absorption cross sections are expected to correctly predict the isotope~~  
17 ~~effects from  $\text{SO}_2$  photolysis (in the 190 nm to 220 nm region) but fail to reproduce the isotope~~  
18 ~~effects from  $\text{SO}_2$  photoexcitation (in the 250 nm to 350 nm region). This is due to the~~  
19 ~~differences in the photophysics and photochemistry between the photolysis region (190 nm to~~  
20 ~~220 nm) and the photoexcitation region (250 nm to 350 nm) – two absorption regions,~~  
21 ~~which result in suggest~~ different mechanisms for MIF formation, [as discussed previously](#)  
22 (Whitehill and Ono, 2012; Ono et al., 2013; Whitehill et al., 2013).

23 In the 165 nm to 235 nm wavelength region,  $\text{SO}_2$  photolysis occurs through predissociation  
24 from the bound  $\tilde{C}(^1B_2)$  state. Near the dissociation threshold of 218.7 nm (Becker et al.,  
25 1995), the quantum yield of photolysis is less than unity, although it increases to greater than  
26 0.99 at wavelengths shorter than 215 nm (Katagiri et al., 1997). In the region where the  
27 quantum yield is close to unity (i.e. less than 215 nm), the isotope effects due to  $\text{SO}_2$   
28 photolysis should be determined entirely by the differences in the absorption cross-sections  
29 between the different isotopologues of  $\text{SO}_2$  (e.g., by isotopologue specific Franck-Condon  
30 coupling; Danielache et al., 2008) and optical screening effects under high  $\text{SO}_2$  column

1 densities (Lyons, 2007, 2008; Ono et al., 2013). In the narrow spectral region from 215 nm to  
2 218.7 nm, where the quantum yield of photodissociation varies, it is possible that quantum  
3 yield differences between isotopologues could potentially produce additional isotope effects  
4 beyond those predicted from absorption cross-sections. However, in this region,  
5 photodissociation occurs primarily via vibronic mixing of the  $\tilde{C}({}^1B_2)$  state levels with the  
6 dissociative continuum of the electronic ground,  $\tilde{X}({}^1A_1)$  state (Katagiri et al., 1997). Due to the  
7 high density of vibronic levels for the  $\tilde{X}({}^1A_1)$  state, it is unlikely that there will be significant  
8 isotope effects in the coupling strength between the  $\tilde{C}({}^1B_2)$  and  $\tilde{X}({}^1A_1)$  states. Dissociation  
9 occurring through mixing with repulsive singlet and triplet states is expected to be small, as is  
10 the nonadiabatic coupling of the  $\tilde{C}({}^1B_2)$  and  $\tilde{D}({}^1A_1)$  states (Tokue and Nanbu, 2010).

11 For laboratory experiments, the observed isotope effects for  $SO_2$  photolysis is a function not  
12 only of differences in the absorption cross-sections (Danielache et al., 2008) but also a  
13 function of the  $SO_2$  column density. This is because the  $SO_2$  absorption cross-section has  
14 significant fine structure, which causes optical screening effects to occur (Lyons, 2007). This  
15 optical screening effect produces larger isotope effects at higher  $SO_2$  column densities (Ono et  
16 al., 2013). In addition to the above effects, there appears to be a total (or bath gas) pressure  
17 effect on  $\Delta^{33}S$  values. This manifests as reduced  $\Delta^{33}S$  values at higher total (i.e. bath gas)  
18 pressures, which is observed with He,  $SO_2$ , and  $N_2$  bath gases (Masterson et al., 2011;  
19 Whitehill and Ono, 2012; Ono et al., 2013). The mechanism responsible for these pressure  
20 effects is still uncertain, but it could suggest that  $^{33}SO_2$  has a longer excited-state lifetime  
21 prior to dissociation than the other isotopologues.

22  $SO_2$  photoexcitation in the 250 nm to 350 nm absorption region also produces absorption-based  
23 isotope effects due to differences in cross-sections and self-shielding. In addition, it produces  
24 isotope effects by a completely different mechanism.  $SO_2$  photoexcitation in the 250 nm to  
25 350 nm region occurs by initial excitation into a coupled  $\tilde{A}({}^1A_2)/\tilde{B}({}^1B_1)$  singlet excited state  
26 that undergoes intersystem crossing to the photochemically active triplet  $\tilde{a}({}^3B_1)$  state (Xie et  
27 al., 2013; Lévêque et al., 2014). Unlike  $SO_2$  photolysis, where the quantum yield of reaction  
28 (i.e. photolysis) is near unity, the quantum yield for intersystem crossing between the singlet  
29 and triplet states is highly variable and state-dependent. Due to the relatively low density of  
30 states in the crossing region ( $\tilde{A}({}^1A_2) \rightarrow \tilde{a}({}^3B_1)$ ), the branching between quenching to the ground  
31 state and intersystem crossing to the triplet state will be a strong function of isotope  
32 substitution. Whitehill et al. (2013) argue that this isotope selective intersystem crossing as

1 the origin of ~~most part~~ of the isotope effects in photochemical products following  
2  $\text{SO}_2$  photoexcitation in the 250 nm to 350 nm absorption region.

3 Photoexcitation of  $\text{SO}_2$  in the presence of  $\text{O}_2$  produces sulfate with both positive  $\Delta^{33}\text{S}$  and  
4 positive  $\Delta^{36}\text{S}$  signals, similar to the organic sulfur observed in Whitehill et al. (2013) and the  
5 elemental sulfur in Whitehill and Ono (2012). This suggests that the anomalous isotope  
6 signatures observed from photoexcitation in previous studies are a result of the  
7 ~~photophysics and photochemistry~~ of excited-state  $\text{SO}_2$  rather than the ~~photo~~chemistry of  
8 subsequent reactions (i.e., the chemistry with acetylene). Our experimental results show  
9 significant discrepancy with isotope effects predicted by isotopologue-specific absorption  
10 cross-sections (Danielache et al., 2012; Hattori et al., 2013) for the 250 nm to 320 nm region  
11 (Whitehill et al., 2013). This is expected if isotope selective intersystem crossing is  
12 ~~everprinting contributing to~~ the isotope signals ~~produced by~~ in addition to cross section  
13 differences ~~and shielding effects~~.

#### 14 4.2 Temperature effects on $\text{SO}_2$ photolysis

15 Lyons (2007, 2008) presented isotopologue-specific absorption cross-sections for  $\text{SO}_2$  in the  
16 190 nm to 220 nm absorption region by shifting the measured  $^{32}\text{SO}_2$  absorption cross-sections  
17 of Freeman et al. (1984) by an amount based on the calculated isotope shifts of Ran et al.  
18 (2007). It has been unclear whether these absorption cross-sections can correctly predict the  
19 isotope effects due to  $\text{SO}_2$  photolysis (Danielache et al. 2008), as they include only isotope  
20 shifts and not other potential differences among isotopologues. Previous comparisons with  
21 experimental data showed significant discrepancies (i.e. a factor of ~2 in  $\delta^{34}\text{S}$  values) between  
22 experimental data and that predicted by the Lyons (2007, 2008) cross-sections (Whitehill and  
23 Ono, 2012; Ono et al., 2013). Such discrepancies were attributed to the difference in  
24 temperature between the Lyons (2007, 2008) cross-sections, which are based on cross-  
25 sections measured at 213 K (Freeman et al., 1984) and the temperature of the experiments  
26 (298 K). Given the new temperature data in the present study, it is possible to compare  
27 calculations based on the Lyons (2007, 2008) cross-sections with temperature-dependent  
28 experimental isotope data. Calculations were performed as described in previous papers  
29 (Whitehill and Ono, 2012; Ono et al., 2013) and are compared to experimental data in Figure  
30 5.

1 Excellent agreement with the Lyons (2007,2008) cross-sections can be seen when the  
2 observed temperature dependence on  $\delta^{34}\text{S}$  are extrapolated back to 213 K. A similar strong  
3 agreement is also seen in the  $\Delta^{36}\text{S}$  values. This new data fills in the major gap between  
4 predictions based on the Lyons (2007, 2008) cross-sections and the room-temperature  
5 experimental data, and provides further support to an optical origin of mass-independent  
6 fractionation during  $\text{SO}_2$  photolysis under laboratory conditions (Ono et al., 2013).

7 Despite the strong agreement for  $\delta^{34}\text{S}$  and  $\Delta^{36}\text{S}$  values, the Lyons (2007, 2008) cross-sections  
8 over-predict the magnitude of the mass-independent isotope anomaly in  $^{33}\text{S}$  (i.e.  $\Delta^{33}\text{S}$  values)  
9 when compared with experimental data. There are several possible explanations for this. One  
10 reason is that there are significant differences between the actual cross-sections and those  
11 predicted by shifting the  $^{32}\text{SO}_2$  cross-sections for  $^{33}\text{SO}_2$ . Measurements by Danielache et al.  
12 (2008) at room temperature suggest that there are some differences between the isotopologue-  
13 specific absorption cross-sections aside from just the spectral shifts accounted for by Lyons  
14 (2007, 2008). A second possibility is that the high total pressure (101.3 kPa, including the  $\text{N}_2$   
15 bath gas) of the experiments caused a decrease in the  $\Delta^{33}\text{S}$  value relative to values observed at  
16 lower total pressures. It has been previously observed (Masterson et al., 2011; Whitehill and  
17 Ono, 2012; Ono et al., 2013) that  $\Delta^{33}\text{S}$  values decrease in the presence of high bath gas  
18 pressures. This pressure quenching effect is most noticeable for  $\Delta^{33}\text{S}$  and does not affect  $\delta^{34}\text{S}$   
19 or  $\Delta^{36}\text{S}$  values as strongly.

20 The Lyons (2007, 2008) cross sections are semi-empirical in that they take the measured  
21  $^{32}\text{SO}_2$  cross-sections of Freeman et al. (1984) and shift them using theoretical isotope shifts  
22 predicted by Ran et al. (2007). Although the Lyons (2007, 2008) cross-sections are not  
23 necessarily accurate,

24 ~~We that~~ the Lyons (2007, 2008) cross sections seem to~~en~~ accurately predict the isotope  
25 effects during  $\text{SO}_2$  photolysis under low temperature (ca. 213 K) conditions, such as those in  
26 the stratosphere.~~z~~

27 ~~Conversely, cross sections measured at room temperature (e.g., Danielache et al., 2008) will~~  
28 ~~underestimate  $\delta^{34}\text{S}$  fractionations when applied to stratospheric conditions.~~

#### 29 **4.3 Constraining the rate of the $\text{SO} + \text{O}_2 + \text{M}$ reaction using product formation**

30 Our results demonstrate that photolysis of  $\text{SO}_2$  in the presence of molecular oxygen ( $\text{O}_2$ )  
31 produces large amounts of sulfate with considerable mass-independent sulfur isotope

1 anomalies. In our experimental system, there are three dominant pathways for  $\text{SO}_3$   
2 formation: OH oxidation of  $\text{SO}_2$  (reactions R1 + R2, if water is present),  $\text{O}_2$  oxidation of  $\text{SO}$   
3 from  $\text{SO}_2$  photolysis (reactions R4 + R6), and O oxidation of  $\text{SO}_2$  via



5 OH and O oxidation of  $\text{SO}_2$  (reactions R1 and R7) are mass dependent (Harris et al., 2012;  
6 Whitehill and Ono, 2012; Ono et al., 2013). However, oxidation of  $\text{SO}$  via R6 will trap the  
7 isotopic composition of  $\text{SO}$  as  $\text{SO}_3$  and carry the mass-independent sulfur isotope signature  
8 from  $\text{SO}_2$  photolysis (R4).

9 We performed a series of experiments at a total pressure of 101.3 kPa, a flow rate of  $6.67 \text{ cm}^3$   
10  $\text{s}^{-1}$  (400 sccm) and an  $\text{SO}_2$  partial pressure of 0.127 kPa (Table 4; Figure 6). The partial  
11 pressure of molecular oxygen was varied from 0 kPa to 19.8 kPa (0 % to 19.5%  $\text{O}_2$ ). In all  
12 experiments,  $\text{SO}_2$  was photolyzed via R4. In the experiments with no oxygen, both elemental  
13 sulfur ( $\text{S}^0$ ) and  $\text{SO}_3$  aerosols were formed, with the elemental sulfur (S and related species)  
14 formed from  $\text{SO}$  via:



16  $\text{SO}$  photolysis is expected to be a minor source of S compared to R8. In the absence of  
17 oxygen,  $\text{SO}_3$  is formed primarily via O oxidation of  $\text{SO}_2$  (R7), which is mass dependent (Ono  
18 et al., 2013).

19 At 5.1 kPa  $\text{O}_2$  and above, elemental sulfur formation was shut off and  $\text{SO}_3$  was the major  
20 product. Under these conditions, oxidation of  $\text{SO}$  (to  $\text{SO}_2$  or  $\text{SO}_3$  via R5 or R6) competes  
21 with  $\text{SO}$  disproportionation (R8).

22 By comparing the  $\Delta^{33}\text{S}$  value of elemental sulfur in the absence of  $\text{O}_2$  (0 kPa  $\text{O}_2$ ) with the  
23  $\Delta^{33}\text{S}$  value of sulfate in the presence of  $\text{O}_2$  (5.1 kPa to 19.8 kPa  $\text{O}_2$ ), it is possible to estimate  
24 the fraction of sulfate formed through R6. In particular,

25 
$$f_{\text{R6}} = \frac{\Delta^{33}\text{S}_{\text{sulfate, with } \text{O}_2}}{\Delta^{33}\text{S}_{\text{S}^0, \text{no } \text{O}_2}}$$
 (5)

26 | **Where**  $f_{\text{R6}}$  is the fraction of total  $\text{SO}_3$  formed that comes from reaction R6. Given the  
27 product yields (Table 4), the time each experiment was run, and the volume of the reaction  
28 cell (approximately  $325 \text{ cm}^3$ ), the sulfate formation rate per unit volume per unit time can be  
29 calculated. In the experiments with 5.1 kPa to 19.8 kPa  $\text{O}_2$ , the sulfate formation rates were

1 between  $5.3 \times 10^{12}$  molecules  $\text{cm}^{-3} \text{ s}^{-1}$  and  $1.2 \times 10^{13}$  molecules  $\text{cm}^{-3} \text{ s}^{-1}$ . Combining this with  
2 the  $f_{R6}$  values calculated from equation 5, we can estimate for the rate of sulfate formation  
3 from reaction R6 under our experimental conditions. This gave a rate for reaction 6 of  
4  $3.6 \times 10^{12}$  molecules  $\text{cm}^{-3} \text{ s}^{-1}$  to  $6.6 \times 10^{12}$  molecules  $\text{cm}^{-3} \text{ s}^{-1}$ . Assuming R6 is a termolecular  
5 reaction, the rate for R6 can be written as:

6 rate R6 =  $k_{R6}[\text{SO}][\text{O}_2][\text{M}]$  (6)

7 where  $k_{R6}$  is the termolecular rate constant for reaction R6 and  $[\text{SO}]$ ,  $[\text{O}_2]$  and  $[\text{M}]$  are the  
8 concentrations of SO, O<sub>2</sub> and total third body gases (M = N<sub>2</sub>, O<sub>2</sub>) in the reaction cell. In  
9 equation (6), the  $[\text{O}_2]$  and  $[\text{M}]$  terms are known from the experimental conditions. The  $[\text{SO}]$   
10 term is estimated by assuming a photochemical steady state for SO in the cell. SO production  
11 via Reaction R4 is balanced by SO destruction via Reactions R5 and R6. This gives us a  
12 steady state SO concentration of:

13  $[\text{SO}] = \frac{J_{\text{SO}_2}[\text{SO}_2]}{k_{R5}[\text{O}_2] + k_{R6}[\text{O}_2][\text{M}]}$  (7)

14 where  $J_{\text{SO}_2}$  is the photolysis rate constant for R4. This photolysis rate constant was calculated  
15 assuming a spectral irradiance for our 150 W Xe arc lamp of:

16  $F_0 / \text{mW nm}^{-1} = 0.11 \cdot 1.6 \cdot (14 - 9 \cdot \exp(-0.013 \cdot (\lambda / \text{nm} - 200)))$  (8)

17 where  $F_0$  is the spectral irradiance of the xenon lamp at wavelength  $\lambda$  (Ono et al., 2013). This  
18 flux might be modified slightly as a function of the distance between the cell and the lamp,  
19 due to interferences from the absorption of oxygen. However, sensitivity studies performed  
20 here and previously (Whitehill and Ono, 2012) suggest that the effect of the oxygen  
21 absorption on the total SO<sub>2</sub> photolysis rate is minor compared to the uncertainty in the lamp  
22 photon flux. The lamp photon flux data was determined from the manufacturer's data and  
23 uncertainty estimates were not available. Despite this, the function used by Ono et al. (2013)  
24 (Equation 8) was used to obtain an estimate for the total SO<sub>2</sub> photolysis rate.

25 The spectral irradiance of the lamp was used to calculate the photon flux entering the cell,  
26 accounting for absorption of the cell windows from measured transmission data. The SO<sub>2</sub>  
27 absorption cross-sections of Manatt and Lane (1993) were used to calculate the photolysis  
28 rate in the cell, accounting for optical screening effects from SO<sub>2</sub> and O<sub>2</sub> within the cell. With  
29 an SO<sub>2</sub> partial pressure of 0.127 kPa, this provided a photolysis rate constant of  $J_{\text{SO}_2} = 5.2 \times 10^{-3}$   
30  $\text{s}^{-1}$ . The rate constant for reaction R5 is  $k_{R5} = 8.0 \times 10^{-17} \text{ cm}^3 \text{ molecule}^{-1} \text{ s}^{-1}$  (Sander et al.,

1 2011) at room temperature (298 K). Using these values and equations (6) and (7), the rate  
2 constant for R6 ( $k_{R6}$ ) was calculated iteratively. Calculated rate constants ranged from  $k_{R6} =$   
3  $7.3 \times 10^{-38} \text{ cm}^6 \text{ molecule}^{-2} \text{ s}^{-1}$  to  $k_{R6} = 1.4 \times 10^{-37} \text{ cm}^6 \text{ molecule}^{-2} \text{ s}^{-1}$ , with an average value of  $k_{R6}$   
4  $= 1.1 \times 10^{-37} \text{ cm}^6 \text{ molecule}^{-2} \text{ s}^{-1}$  (Table 4). This rate estimate is consistent with the upper bound  
5 on  $k_{R6} \leq 1 \times 10^{-36} \text{ cm}^6 \text{ molecule}^{-2} \text{ s}^{-1}$  by Black et al. (1982).

6 The calculated rate constant ( $k_{R6}$ ) appears to decrease at 19.8 kPa O<sub>2</sub> compared with  
7 the calculated rate for lower  $pO_2$  values. It is unclear why this behavior is observed. The  
8 relatively strong agreement for the other conditions strengthens our confidence that the model  
9 is robust.

10 TheThe derived rate constant carries ~~a large amount of~~ uncertainty due to a number of  
11 sources of error in the rate calculation. One source of error in the calculation is in the spectral  
12 irradiance of the xenon lamp, which was fit from the manufacturer's literature and not directly  
13 measured. Because the spectral irradiance is likely to change over the lamp's lifetime, the  
14 actual spectral irradiance at the time the experiments were performed might be different than  
15 the values calculated here. As the spectral irradiance in the high-energy side of the ultraviolet  
16 (190 nm to 220 nm) is likely to decrease over the course of the lamp's lifetime, this makes the  
17 calculated SO<sub>2</sub> photolysis rate (and resulting SO number density) an upper bound. Reducing  
18 the SO<sub>2</sub> photolysis rate increases the effective rate constant. A second source of error is the  
19 assumption that we trapped 100% of the SO<sub>3</sub> formed as sulfate. It is possible that some  
20 fraction of the SO<sub>3</sub> remained in the gas phase and did not condense as aerosol particles. A  
21 third source of error is the assumption that the reaction R6 behaves as a termolecular reaction  
22 despite the high total pressure (101.3 kPa) of the system. It is possible that the reaction is  
23 saturated at (or near) this pressure and is thus behaving as an effective bimolecular reaction.  
24 In any of these three cases, the estimate of the rate constant for reaction R6 would be a lower  
25 bound on the actual termolecular rate constant.

Formatted: Indent: First line: 0.49"

26 It is also important to consider the impact of water vapor within the system. Although  
27 attempts were made to minimize the amount of water vapor in the system, there was almost  
28 certainly some water vapor in the system during our experiments. This is evidenced by  
29 the visible formation of sulfate aerosols from SO<sub>3</sub> during the experiments. Unfortunately, we  
30 did not have the analytical capability to quantitatively constrain the amount of water vapor in  
31 the system during the experiments. The Zero Air and Nitrogen used as a source of gas to the  
32 cell has a maximum of 3 ppm H<sub>2</sub>O (by volume), but there could be additional water absorbed

1 onto the surfaces of the system while the cell is disassembled. We assume 100% of the  $\text{SO}_3$   
2 was trapped as sulfate, giving a lower bound estimate on the rate of reaction R6.

3 **4.4 Constraining the rate of the  $\text{SO} + \text{O}_2 + \text{M} \rightarrow \text{SO}_3 + \text{M}$  reaction using a kinetic model**

4 To further constrain the rate of R6 (the  $\text{SO} + \text{O}_2 + \text{M} \rightarrow \text{SO}_3 + \text{M}$  reaction), we constructed a  
5 kinetic model of the chemistry occurring within the cell. We used the same data and  
6 conditions as Section 4.3, but explicitly modeled the chemistry occurring within the system.  
7  $\text{SO}_2$  photolysis rates were calculated as discussed in Section 4.3, using the cross sections of  
8 Manatt and Lane (1993). Oxygen and ozone photolysis rates were calculated using the cross-  
9 sections Yoshino et al. (1988, 1992) for  $\text{O}_2$  and Molina and Molina(1986) for  $\text{O}_3$ . Quantum  
10 yields for  $\text{O}(\text{^1D})$  versus  $\text{O}(\text{^3P})$  formation from  $\text{O}_3$  photolysis were parameterized based on the  
11 recommendation of DeMore et al. (1997). Photolysis rates for  $\text{HO}_2$  and  $\text{H}_2\text{O}_2$  were calculated  
12 using the recommended cross-sections of Sander et al. (2011).  $\text{HO}_2$  photolysis was assumed  
13 to produce  $\text{O}(\text{^1D})$  and  $\text{OH}$  as products, and  $\text{H}_2\text{O}_2$  photolysis was assumed to produce  $2\text{OH}$ .  
14  $\text{O}(\text{^1D})$  formed from  $\text{O}_3$  photolysis was assumed to be instantaneously quenched by  $\text{N}_2$  and  
15  $\text{O}_2$  to  $\text{O}(\text{^3P})$  and not significantly affect the chemistry of the system.

16 The rate constants and their sourcesReactions considered, rate constants for those reactions,  
17 and the sources for the rate constants are given in Table 9. When possible, effective second-  
18 order rate constants (calculated assuming  $T = 298 \text{ K}$  and  $[\text{M}] = 2.5 \times 10^{19} \text{ molecule cm}^{-3}$ ) were  
19 used for termolecular reactions. Initial guesses were made for the concentration of species  
20 within the system. The system was assumed to be in photochemical steady state and solved  
21 iteratively until convergence. Comparisons were made between the data and the calculations  
22 for ~~both~~  $f_{\text{R6}}$  values (Equation 5) ~~as well as total product ( $\text{SO}_3$ ) formation rates.~~ Simulations  
23 ~~were~~ performed with values of  $k_{\text{R6}}$  ~~between of~~  $1.0 \times 10^{-37} \text{ cm}^6 \text{ molecule}^{-2} \text{ s}^{-1}$  ~~and~~  $1.0 \times 10^{-36} \text{ cm}^6$   
24  $\text{molecule}^{-2} \text{ s}^{-1}$  ~~and~~  $1.0 \times 10^{-35} \text{ cm}^6 \text{ molecule}^{-2} \text{ s}^{-1}$ . Since the amount of water vapor in the  
25 system was not constrained experimentally, three simulations were performed, with  $\text{H}_2\text{O}$   
26 concentrations of 0 ppm (by volume), 10 ppm (by volume), and 100 ppm (by volume), which  
27 spans a range of reasonable estimates for water vapor concentration in the system. Although  
28 water vapor in the bath gas ( $\text{N}_2$  and  $\text{N}_2/\text{O}_2$ ) are less than 3 ppm (by volume), additional water  
29 could be absorbed onto the inner surfaces of the cell and released during the  
30 experiment. Results for 0 ppm  $\text{H}_2\text{O}$  and 10 ppm  $\text{H}_2\text{O}$  predict rates for reaction R6 on the order  
31 ~~of  $10^{-36} \text{ cm}^6 \text{ molecule}^{-2} \text{ s}^{-1}$ , with predictions for 100 ppm  $\text{H}_2\text{O}$  being slightly higher.~~

1 There is a discrepancy between model predictions and the observed experimental behavior.  
2 In particular, lower O<sub>2</sub> fractions produce higher estimated rates and vice versa. In addition, the  
3 model predicts rates mostly higher than the previous upper bound on the rate calculated by  
4 Black et al. (1982) of 10<sup>-36</sup> cm<sup>6</sup> molecule<sup>-2</sup> s<sup>-1</sup>. Helium was used as a bath gas for the Black et  
5 al. (1982) experiments, as compared with nitrogen or nitrogen / oxygen used as the bath gas  
6 here. Nitrogen (N<sub>2</sub>) and oxygen (O<sub>2</sub>) are a more efficient third body quenchers than helium.  
7 Thus, the rate of the termolecular reaction with nitrogen (or nitrogen/oxygen) as a bath gas  
8 could be higher than the maximum constraint suggested by Black et al. (1982). There is also  
9 an order of magnitude discrepancy between the predictions here and those in Section 4.3, with  
10 those in Section 4.3 being an order of magnitude smaller than those in Section 4.4. This could  
11 be based on the assumption that 100% of the SO<sub>3</sub> was trapped as sulfate in Section 4.3,  
12 whereas the actual amount might be less than that (implying a higher rate than predicted in  
13 Section 4.3). However, the model predicts rate constants within an order of magnitude of  
14 previous constraints from the literature (Black et al., 1982) and Section 4.3. Based on this  
15 work, we estimate the rate of this reaction to be on the order of 10<sup>-37</sup> cm<sup>6</sup> molecule<sup>-2</sup> s<sup>-1</sup> to 10<sup>-36</sup>  
16 cm<sup>6</sup> molecule<sup>-2</sup> s<sup>-1</sup>. Future work is necessary to better constrain the rate of this reaction.  
17 The observed  $kR6$  value (equation 5) is best fit by the  $kR6$  between  $2 \times 10^{-37}$  cm<sup>6</sup> molecule<sup>-2</sup>  
18 s<sup>-1</sup> and  $10 \times 10^{-37}$  cm<sup>6</sup> molecule<sup>-2</sup> s<sup>-1</sup> (Figure 7, left). The yield of SO<sub>3</sub> indicates a lower  
19 rate constant of less than  $1 \times 10^{-37}$  cm<sup>6</sup> molecule<sup>-2</sup> s<sup>-1</sup> to  $3 \times 10^{-37}$  cm<sup>6</sup> molecule<sup>-2</sup> s<sup>-1</sup>,  
20 potentially reflecting low recovery of SO<sub>3</sub> in our experiments (Figure 7, right). Nonetheless,  
21 this range of results is consistent with the rate estimate obtained in Section 4.3. Thus, our best  
22 estimate for the rate of reaction R6 is somewhere between  $1.0 \times 10^{-37}$  cm<sup>6</sup> molecule<sup>-2</sup> s<sup>-1</sup> and  
23  $1.0 \times 10^{-36}$  cm<sup>6</sup> molecule<sup>-2</sup> s<sup>-1</sup>. As discussed in Section 4.3, the model is sensitive to the SO<sub>2</sub>  
24 photolysis rate, which depends upon the lamp spectrum.

Formatted: Subscript

Formatted: Superscript

Formatted: Superscript

Formatted: Superscript

Formatted: Superscript

Formatted: Not Superscript/ Subscript

Formatted: Subscript

## 4.5 Exploring the potential energy surfaces of the SO + O<sub>2</sub> reactions

26 The experimental evidence presented above suggests the formation of SO<sub>3</sub> via the SO+O<sub>2</sub>  
27 reaction. Our theoretical analysis shows that the singlet PES is associated with the ground  
28 state of the SO<sub>3</sub> molecule, and thus is the primary surface related to the SO(<sup>3</sup>Σ<sup>+</sup>) + O<sub>2</sub>(<sup>3</sup>Σ<sub>g</sub><sup>-</sup>)  
29 →SO<sub>3</sub>(<sup>1</sup>A<sub>1</sub>) reaction (Figure 4). As shown in Table 7, four isomers of SO<sub>3</sub> are located in the  
30 singlet PES. It is predicted that the D<sub>3h</sub>SO<sub>3</sub> molecule isomer is the global minimum, followed  
31 by the cyclic-OSOO. There are two shallower wells, denoted as trans-OSOO and cis-OSOO,

1 at the CASPT2 and UCCSD(T)-F12a levels, but they [seem-appear](#) to be energetically higher  
2 than the  $\text{SO}(\text{3}\Sigma^-) + \text{O}_2(\text{3}\Sigma_g^-)$  asymptote at the B3LYP and CASSCF levels. No barrier was  
3 found for the formation of either trans-OSOO or cis-OSOO, but there is a barrier for the  
4 isomerization and the barrier height depends upon the level of the ab-initio calculation. The  
5 rate-determining barrier for the  $\text{SO}(\text{3}\Sigma^-) + \text{O}_2(\text{3}\Sigma_g^-) \rightarrow \text{SO}_3(\text{1}A_1)$  reaction is the one connecting  
6 [the](#)-cyclic-OSOO and  $\text{SO}_3$ . The lowest barrier height for this reaction (given by CASPT2) is  
7 56.6 kJ mole<sup>-1</sup>. Using the partition function at the B3LYP level, a conventional transition-  
8 state theory rate calculation predicts a pressure-saturated (i.e. effective bimolecular) thermal  
9 rate constant for reaction R6 at 298K of  $2.7 \times 10^{-24}$  cm<sup>3</sup> molecule<sup>-1</sup> s<sup>-1</sup>. This is about eight  
10 orders of magnitude lower than the experimental rate constant for reaction R5 ( $8.0 \times 10^{-17}$  cm<sup>3</sup>  
11 molecule<sup>-1</sup> s<sup>-1</sup>, Sander et al., 2011), and about six orders of magnitude lower than the  
12 minimum effective second-order rate constant for reaction R6 at 101.3 kPa total pressure  
13 (about  $2.5 \times 10^{-18}$  cm<sup>3</sup> molecule<sup>-1</sup> s<sup>-1</sup>, calculated assuming  $k_{R6} = 1.0 \times 10^{-37}$  cm<sup>6</sup> molecule<sup>-1</sup> s<sup>-1</sup> and  
14  $[\text{M}] = 2.5 \times 10^{19}$ ). We thus conclude that the  $\text{SO}(\text{3}\Sigma^-) + \text{O}_2(\text{3}\Sigma_g^-) \rightarrow \text{SO}_2(\text{1}A_1) + \text{O}(\text{3}P)$  reaction  
15 cannot occur on the singlet surface without invoking the spin-forbidden intersystem crossing  
16 between the singlet and triplet surfaces.

17 The triplet PES is very different from the singlet PES with regard to the energy of each  $\text{SO}_3$   
18 isomer (Figure 4; Table 8). The global minimum moves to the cyclic-OSOO [isomer](#), which  
19 has a similar geometry to the singlet (ground) state counterpart but with different bond  
20 lengths. On the other hand,  $\text{SO}_3(\text{3}A_1)$  becomes highly unfavorable; for example, it is 75.14 kJ  
21 mole<sup>-1</sup> higher than the  $\text{SO} + \text{O}_2$  reactants [at](#) the UCCSD(T)-F12a level. The trans-OSOO  
22 complex remains in a planar geometry, in which the O-S-O-O dihedral angle is 180°;  
23 however, the cis-OSOO complex was found to be out-of-plane, in which the O-S-O-O  
24 dihedral angle is about 74°. We still use “cis-OSOO” to denote this isomer for convenience.  
25 Unlike the singlet PES, trans-OSOO and cis-OSOO share the same transition state for the  
26 isomerization to cyclic-OSOO. This process represents the rate-limiting step for the reaction  
27 on the triplet surface. The barrier height is 67.86 kJ mole<sup>-1</sup> at the UCCSD(T)-F12a level,  
28 which is still high. In the adiabatic picture, the  $\text{SO}(\text{3}\Sigma^-) + \text{O}_2(\text{3}\Sigma_g^-) \rightarrow \text{SO}_2(\text{1}A_1) + \text{O}(\text{3}P)$   
29 reaction on the triplet PES has a rate constant of  $2.7 \times 10^{-25}$  cm<sup>3</sup> molecule<sup>-1</sup> s<sup>-1</sup> at 298 K,  
30 estimated using transition-state theory. This is still considerably slower than the  
31 experimentally measured rate constant for reaction R5.

1 It is clear that a single PES is unable to reproduce the experimental data for reactions R5 and  
2 R6. ~~The deviation is rather large and cannot be attributed to tunneling effects.~~ In order to  
3 explore the possibility of intersystem crossing, two adiabatic minimum energy pathways on  
4 both spin states are shown in Figure 4 and the energies are extracted at the UCCSD(T)-  
5 F12a//B3LYP level. There are several places that the two PESs cross each other, and a spin  
6 flip could happen in the region near the cyclic-OSOO isomer due to the fact that ~~the cyclic~~  
7 ~~OSOO~~-isomer on both PESs has nearly the same energy. A possible non-adiabatic reaction  
8 pathway is depicted in Figure 4 by the green solid lines connecting every two stationary  
9 points. Specifically, for the  $\text{SO}({}^3\Sigma^-) + \text{O}_2({}^3\Sigma_g^-) \rightarrow \text{SO}_3({}^1\text{A}_1)$  reaction, the two reactants first  
10 approach each other to form cyclic-OSOO on the singlet PES, and jump to the triplet PES to  
11 avoid the high barrier region, followed by back transition to the singlet state to form the  $\text{SO}_3$   
12 product. For the  $\text{SO}({}^3\Sigma^-) + \text{O}_2({}^3\Sigma_g^-) \rightarrow \text{SO}_2({}^1\text{A}_1) + \text{O}({}^3\text{P})$  reaction, the intermediate cyclic-  
13 OSOO may be generated on the singlet PES, followed by intersystem crossing from the  
14 singlet to triplet surface and then reach the products without overcoming a high barrier.  
15 Indeed, several different mechanisms introducing the intersystem crossing have been  
16 proposed by other authors for the  $\text{SO}_3 \rightarrow \text{SO}_2 + \text{O}$  reactions (Davis, 1974; Westenberg and  
17 Dehaas, 1975; Astholz et al., 1979), thanks to the relatively large spin-orbit coupling of the  
18 heavy sulfur. The barrier associated with the intersystem crossing pathway seems to be  
19 consistent with the fast rate of R5, and supports the facile formation of  $\text{SO}_3$ .

20 Unfortunately, rate constants involving the intersystem crossing cannot be readily determined  
21 from the current calculations, without global PESs for both spin states and the coupling  
22 between them would be required for a complete calculation. Such a goal can only be  
23 achieved by a multi-reference method or configuration interaction method, which is infeasible  
24 at the current level. On-the-fly transition state surface hopping calculations would present an  
25 alternative method to derive rate constants without the need for global potential energy  
26 surfaces and should be pursued in future work.

27 **4.6 Contribution of the  $\text{SO} + \text{O}_2 + \text{M}$  reaction to sulfate formation in the**  
28 **stratosphere**

29 To determine the significance of the reaction R6 to sulfate formation in the stratosphere, we  
30 compared the rate of sulfate formation via R6 to that formed via OH oxidation of  $\text{SO}_2$   
31 (reaction R1) and O oxidation of  $\text{SO}_2$  (reaction R7) under a select set of atmospheric

1 conditions. We assumed an atmospheric temperature and pressure profile of the U.S. Standard  
2 Atmosphere 1976 (COESA, 1976) and noon-time O, OH, and O<sub>3</sub> concentrations given by  
3 DeMore et al. (1997). Spectral photon flux in the 180 nm to 220 nm region was calculated as  
4 a function of altitude for a solar zenith angle of 40° by assuming the spectral photon irradiance  
5 of Rottman et al. (2006) at the top of the atmosphere and O<sub>2</sub>, O<sub>3</sub>, and CO<sub>2</sub> being the dominant  
6 absorbers. Absorption cross-sections of O<sub>2</sub> (Yoshino et al., 1988, 1992), O<sub>3</sub> (Molina and  
7 Molina, 1986), and CO<sub>2</sub> (Shemansky, 1972) were used with concentration and column density  
8 data for the species to calculate the transmission of the atmosphere to radiation in the 180 nm  
9 to 220 nm absorption region at different altitudes. SO<sub>2</sub> photolysis rate constants ( $J_{SO_2}$ ) were  
10 calculated as a function of altitude using the calculated spectral photon fluxes and the SO<sub>2</sub>  
11 absorption cross-sections of Manatt and Lane (1993).

12 The lifetime of SO with respect to oxidation by O<sub>2</sub> (i.e. R5 and R6) is relatively short (on the  
13 order of seconds), so SO and SO<sub>2</sub> were assumed to be in photochemical steady state, i.e.

$$14 \frac{[SO]}{[SO_2]} = \frac{J_{SO_2}}{k_{R5}[O_2] + k_{R6}[O_2][M]} \quad (9)$$

15 The rate constant  $k_{R5}$  was calculated as a function of altitude (i.e. temperature) based on the  
16 recommendations of Sander et al. (2011).  $k_{R6}$  was varied between  $1.0 \times 10^{-37}$  cm<sup>6</sup> molecule<sup>-2</sup> s<sup>-1</sup>  
17 and  $1.0 \times 10^{-36}$  cm<sup>6</sup> molecule<sup>-2</sup> s<sup>-1</sup> to encompass ~~our range of the order of magnitude~~ rate  
18 estimates from Section 4.3 and 4.4. SO oxidation by other oxidants (O<sub>3</sub>, O, NO<sub>3</sub>, etc.) was  
19 assumed to be minor compared to oxidation by O<sub>2</sub> given the minor concentration of most of  
20 these species compared with that of O<sub>2</sub>. Using the [SO] to [SO<sub>2</sub>] ratio, the rates of R1, R7,  
21 and R6 can be compared. Assuming these three reactions are the dominant source of SO<sub>3</sub>  
22 (and subsequently sulfate) in the stratosphere, the fraction of sulfate from reaction R6 ( $f_{SO}$ )  
23 can be calculated as:

$$24 f_{SO} = \frac{\frac{[SO]}{[SO_2]} \cdot k_{R6}[O_2][M]}{k_{SO_2+OH}[OH] + k_{SO_2+O}[O] + \frac{[SO]}{[SO_2]} \cdot k_{R6}[O_2][M]} \quad (10)$$

25 The rate constants  $k_{SO_2+OH}$  and  $k_{SO_2+O}$  are the effective bimolecular rate constants for reactions  
26 R1 and R7, as recommended by Sander et al. (2011).  $f_{SO}$  values were calculated for a 40°  
27 solar zenith angle (local noon at 40°N latitude and a 0° solar declination angle) and are shown  
28 in Figure 8. Given that SO, OH, and O(<sup>3</sup>P) are all formed as a result of photochemistry, they

1 should have similar daily cycles. As a result, the  $f_{SO}$  values calculated for local noon should  
2 be similar to daily average  $f_{SO}$  values.

3 As seen in Figure 8, the lower **bound** estimate for  $k_{R6}$  ( $1.0 \times 10^{-37}$  cm $^6$  molecule $^{-2}$  s $^{-1}$ ) gives 4%  
4 to 10% of sulfate from R6 between 25 km and 50 km altitude. A faster estimate for  $k_{R6}$  of  
5  $2.0 \times 10^{-37}$  cm $^6$  molecule $^{-2}$  s $^{-1}$  gives 8% to 18% of sulfate from R6 between 25 km and 50 km  
6 altitude. The upper bound estimate for the rate ( $k_{R6} = 1.0 \times 10^{-36}$  cm $^6$  molecule $^{-2}$  s $^{-1}$ , from  
7 Black et al., 1982) suggests that over 45% of sulfate could be coming from R6 between 31 km  
8 and 34 km altitude and is probably unrealistic. The contribution from R6 depends upon the  
9 amount of photons available for SO<sub>2</sub> photolysis, which increases with altitude because of less  
10 absorption by Schuman-Runge band of O<sub>2</sub> and the Hartley bands of O<sub>3</sub>. The rate of R6  
11 decreases at higher altitude as total number density decrease. The maximum  $f_{SO}$  value, thus,  
12 is between 30 and 35 km (Figure 8).

13 Some insight into the rate can be obtained from SO<sub>2</sub> lifetimes in the stratosphere. Following  
14 the Mt. Pinatubo (1991) eruption, the Total Ozone Mapping Spectrometer (TOMS) data  
15 (Bluth et al., 1992) and Microwave Limb Sounder (MLS) data (Read et al., 1993) were used  
16 to estimate an e-folding time of 33 days to 35 days for SO<sub>2</sub> in the stratosphere. A later  
17 reanalysis of the TOMS data and TIROS Optical Vertical Sounder (TOVS) data (Guo et al.,  
18 2004) reduced this value to 25 days. Bekki and Pyle (1994) modeled the SO<sub>2</sub> decay following  
19 the Mt. Pinatubo eruption, considering R1 as the only sink of SO<sub>2</sub> in the stratosphere. Their  
20 modeled decay times for SO<sub>2</sub> (40 days) are considerably longer than the measured value of 25  
21 days. Bekki and Pyle (1994) attributed this to uncertainties in the OH number densities. The  
22 discrepancy, however, could be explained in part by SO<sub>2</sub> photolysis followed by R6. Inclusion  
23 of the SO<sub>2</sub> photolysis sink would decrease the lifetimes for SO<sub>2</sub> above around 25 km. The  
24 presence of this reaction would also suggest that OH concentrations estimated by Read et al.  
25 (1993) based on SO<sub>2</sub> lifetimes might overestimate OH concentrations above around 25 km  
26 altitude.

27 SO<sub>2</sub> photolysis is self-limiting, as SO<sub>2</sub> photolysis near the top of the volcanic SO<sub>2</sub> plume  
28 absorbs ultraviolet radiation in the range that SO<sub>2</sub> photolysis occurs. As a result, SO<sub>2</sub>  
29 photolysis lower in the eruption cloud is reduced and depends upon the overlying SO<sub>2</sub> column  
30 density. This would potentially reduce the significance of R6 under heavy SO<sub>2</sub> loading.

31 Optical shielding effects increase the magnitude of the isotope effect from SO<sub>2</sub> photolysis  
32 under high SO<sub>2</sub> column densities (Lyons et al., 2007; Ono et al., 2013). Thus, the isotope

1 fractionation occurring in a volcanic cloud is a tradeoff between larger fractionations but  
2 lower photolysis rates at higher column densities versus smaller fractionations but higher  
3 photolysis rates at lower column densities. Although the instantaneous fractionation factors  
4 can be ~~accurately~~ estimated using our results and cross section by Lyons (2007, 2008), the  
5 temporal evolution of isotope signatures of sulfate aerosol will require a model that accurately  
6 incorporates both chemistry and dynamics of stratosphere.

7 Given the large signal produced by  $\text{SO}_2$  photolysis, over 100‰ and 10‰ for  $\delta^{34}\text{S}$  and  $\Delta^{33}\text{S}$   
8 values, respectively (Whitehill and Ono, 2012; Ono et al., 2013), even a 10% contribution  
9 from reaction R5 could make a substantial contribution to the isotope signature of sulfate  
10 formed above circa 25 km altitude. Given the strong similarity in the isotopic signature of  
11 stratospheric sulfate aerosols from volcanic eruptions and those produced during  $\text{SO}_2$   
12 photolysis (Figure 3), it is likely that  $\text{SO}_2$  photolysis plays an important role in the sulfur  
13 isotope budget of stratospheric sulfate aerosols. The initial sulfate formed from  $\text{SO}_2$   
14 photolysis (followed by R6) will contain positive  $\delta^{34}\text{S}$  and  $\Delta^{33}\text{S}$  values and negative  $\Delta^{36}\text{S}$   
15 values. Over time, due to mass balance, the residual  $\text{SO}_2$  will obtain negative  $\delta^{34}\text{S}$  and  $\Delta^{33}\text{S}$   
16 values and positive  $\Delta^{36}\text{S}$  values. This explains the temporal evolution of the isotopic  
17 signatures observed in aerosol samples (for  $\delta^{34}\text{S}$ , Castleman et al., 1974) and ice cores (Baroni  
18 et al., 2007), which goes from positive  $\delta^{34}\text{S}$  and  $\Delta^{33}\text{S}$  values shortly after an eruption to  
19 negative values as time progresses.

20

## 21 **4.7 Insignificance of excited-state photochemistry of $\text{SO}_2$ in the stratosphere**

22 It has been suggested previously (Savarino et al., 2003; Hattori et al., 2013) that excited-state  
23 photochemistry of  $\text{SO}_2$  in the 250 nm to 350 nm absorption region (i.e. the  $\tilde{A}({}^1\text{A}_2)/\tilde{B}({}^1\text{B}_1)$   
24 states) might be ~~important the dominant source of~~ the sulfur isotope ratios in stratospheric  
25 sulfate aerosols. Previous results (Whitehill and Ono, 2012; Whitehill et al., 2013) have  
26 demonstrated that  $\text{SO}_2$  photoexcitation in this region produces mass-independent sulfur  
27 isotope signatures with positive  $\Delta^{36}\text{S}/\Delta^{33}\text{S}$  ratios, as opposed to the negative  $\Delta^{36}\text{S}/\Delta^{33}\text{S}$  ratios  
28 measured for stratospheric sulfate aerosols. This study further demonstrates that  
29  $\text{SO}_2$  photoexcitation in the 250 nm to 350 nm absorption region produces positive  $\Delta^{36}\text{S}/\Delta^{33}\text{S}$   
30 ratios, even at temperatures approaching stratospheric temperatures. Our previous  
31 experiments (Whitehill and Ono, 2012; Whitehill et al., 2013) have been questioned as being

1 inapplicable to the modern atmosphere (Hattori et al., 2013) due to the experimental  
2 conditions (i.e. the addition of C<sub>2</sub>H<sub>2</sub> to trap triplet-state SO<sub>2</sub>). In the present study, we tested  
3 SO<sub>2</sub>photoexcitation with two different longpass filters (250 nm longpass filter and 280 nm  
4 longpass filter) in a N<sub>2</sub>/O<sub>2</sub> bath gas. In all cases, we produced sulfate products with positive  
5  $\Delta^{36}\text{S}/\Delta^{33}\text{S}$  ratios. Therefore, our experiments do not provide support for SO<sub>2</sub>photoexcitation  
6 as ~~the dominant~~ source of the isotope anomalies in modern atmospheric samples.

7 ~~However, contribution from both absorption bands to the isotope effects observed in  
8 stratospheric sulfate aerosols is possible and should be considered further. Despite the strong  
9 correspondence between  $\Delta^{36}\text{S}/\Delta^{33}\text{S}$  ratios in our photolysis experiments and stratospheric  
10 sulfate aerosol samples (Figure 3), the stratospheric sulfate aerosol samples produces a  
11 slightly shallower (less negative)  $\Delta^{36}\text{S}/\Delta^{33}\text{S}$  slope than the majority of our experimental  
12 samples. This could be due in part to the effect of pressure on  $\Delta^{36}\text{S}/\Delta^{33}\text{S}$  ratios (Masterson et  
13 al., 2011), as the one experiment performed at 7.7 kPa total pressure (Table 5) produced a  
14  $\Delta^{36}\text{S}/\Delta^{33}\text{S}$  more similar to the stratospheric sulfate aerosol samples than the experiments  
15 performed at 101.3 kPa total pressure. It could also be due, however, to mixing between the  
16 negative  $\Delta^{36}\text{S}/\Delta^{33}\text{S}$  signatures from SO<sub>2</sub> photolysis and the positive  $\Delta^{36}\text{S}/\Delta^{33}\text{S}$  signatures from  
17 SO<sub>2</sub>photoexcitation. It is critical that future experiments further explore the isotope effects  
18 within these two absorption regions. However, it is also clear that SO<sub>2</sub>photoexcitation alone  
19 is not likely to be responsible for the isotope signatures and that SO<sub>2</sub> photolysis is necessary  
20 as well.~~

#### 21 **4.8 Caveats for Experimental Studies**

22 ~~There are a number of difficulties with directly applying photochemical results from  
23 laboratory studies to processes occurring in the natural environment. One issue is the  
24 difference between the spectral photon flux of the Xe and D<sub>2</sub> arc lamps as compared with the  
25 solar spectrum. Comparisons of data from different light sources (Xe versus D<sub>2</sub> lamps) were  
26 made previously in static photochemical experiments (Whitehill and Ono, 2012) and showed  
27 minor differences depending upon the light source. However, despite the large differences in  
28 the spectral photon flux between the Xe and D<sub>2</sub> light sources, the patterns in the isotope  
29 fractionation (i.e.  $\delta^{34}\text{S}$  versus  $\Delta^{33}\text{S}$  versus  $\Delta^{36}\text{S}$ ) are similar. Both the Xe and D<sub>2</sub> light sources  
30 are broadband, unstructured light sources in the 180 nm to 220 nm absorption region, where  
31 SO<sub>2</sub> photolysis occurs. The solar spectrum, although also broadband, has considerably more  
32 fine structure in the spectrum, due to absorption by other gases such as O<sub>2</sub>. As demonstrated~~

Formatted: Normal, Indent: First line: 0.4"

1 in early  $\text{SO}_2$  photolysis experiments (Farquhar et al. 2001), highly structured light sources  
2 (such as laser light sources) can cause anomalous isotope effects different from those  
3 observed in a broadband regime (Whitehill and Ono, 2012).

4 Unfortunately, the currently available measured absorption cross-sections (Danielache  
5 et al. 2008) do not reproduce the results of photochemical experiments (Whitehill and Ono,  
6 2012). As shown by Ueno et al. (2009), they predict negative  $\Delta^{33}\text{S}$  values from  $\text{SO}_2$   
7 photolysis under reasonable atmospheric conditions. Photochemical experiments show  
8 positive  $\Delta^{33}\text{S}$  values near zero (except in the self-shielding regime; Ono et al., 2013) under  
9 similar conditions. It is also important to note that the magnitude of uncertainties in the cross-  
10 section measurements (on the percent level) are too large to be considered quantitative for that  
11 of mass-independent fractionation observed in these reactions. Future, higher-precision and  
12 higher resolution cross-section measurements should resolve some of these discrepancies and  
13 allow for stratospheric fractionations under solar spectral conditions to be modeled. In the  
14 absence of this data, however, experiments using solar-like spectra (i.e. Xe arc lamp) can  
15 provide a first order constraint on the types of isotope fractionations expected under a solar  
16 regime.

Formatted: Subscript

17 Another major issue with the experiments that was discussed above is the poor control  
18 in the experiments over the amount of water in the system. Due to the fact that experiments  
19 were performed at room temperature rather than at vacuum, it is difficult to put definitive  
20 constraints on the amount of water present in the system. Although attempts were made to  
21 flush the systems with nitrogen (< 3 ppb  $\text{H}_2\text{O}$ ) prior to each experiment, water could be  
22 adsorbed onto the surfaces of the system. The presence of water will cause  $\text{HO}_x$  chemistry to  
23 occur and open up an additional (mass-dependent, Harris et al. 2012) channel for sulfate  
24 formation. The amount of water in the system also affects the amount of  $\text{SO}_3$  that ends up as  
25 sulfate aerosols. This is particularly an issue when attempting to estimate the rate of reactions  
26 in the system (Section 4.3 and 4.4). Differences in the amount of water within the system  
27 during different experiments could explain some of the isotopic variability between replicate  
28 experiments (Tables 4 and 5). Photoexcitation (250 nm to 350 nm) experiments performed in  
29 an identical photochemical system but with the addition of acetylene ( $\text{C}_2\text{H}_2$ ) are not strongly  
30 affected by the presence of trace amounts of water in the system, and showed considerably  
31 better isotopic reproducibility (Whitehill et al. 2013; Table 3) than  $\text{SO}_2$  photolysis  
32 experiments (Ono et al., 2013; Tables 2, 4, and 5). This suggests that variability in trace

Formatted: Subscript

1 amounts of water present in the system could have a significant affect on the isotopic  
2 signatures during SO<sub>2</sub> photolysis, and that water vapor should be carefully controlled in future  
3 experiments.

4

5 **4.84.9 Production and preservation of mass-independent sulfur isotope**  
6 **signatures in ice cores**

7 The results presented in this paper can explain the production and preservation of mass-  
8 independent sulfur isotope signatures in the modern atmosphere. Large volcanic eruptions,  
9 such as Pinatubo (1991) and Agung (1963) inject large amounts of SO<sub>2</sub> into the stratosphere.

10 Both direct injection into higher altitudes (i.e. above around 20 to 25 km) or stratospheric  
11 transport of the SO<sub>2</sub> plume can bring SO<sub>2</sub> to a sufficient altitude for SO<sub>2</sub> photolysis to occur.

12 The process of SO<sub>2</sub> photolysis produces large mass-independent sulfur isotope signatures in  
13 the SO products, particularly when there is high SO<sub>2</sub> loading (and thus optical screening  
14 effects). Reaction of SO with O<sub>2</sub> to produce SO<sub>3</sub> (via R6) provides a pathway for the isotopic  
15 signature of SO to be preserved as SO<sub>3</sub>, which can subsequently form sulfate aerosols. Some  
16 portion of the sulfate aerosols containing the mass-independent sulfur isotope signatures are  
17 transported to polar regions, where they can be deposited in polar precipitation and preserved  
18 in ice core records. A schematic illustration of the process is shown in Figure 9.

19 Some eruptions, despite their stratospheric influence, produce sulfate peaks in ice core records  
20 but do not contain mass-independent sulfur isotope signatures. Such eruptions include Cerro  
21 Hudson (1991, Savarino et al., 2003) and Laki (1783, Lanciki et al., 2012). Schmidt et al.  
22 (2012) discussed this issue previously and concluded that the Laki aerosols deposited in the  
23 Greenland ice cores were predominantly upper tropospheric or lower stratospheric in  
24 origin. Estimates for the height of the Laki (1783) eruption plume are only 15 km (Thordarson  
25 and Self, 2003), which penetrates the stratosphere but is not sufficiently high for SO<sub>2</sub>  
26 photolysis to be a dominant process (Schmidt et al., 2012). Due to the higher latitude of the  
27 eruption, transport processes are unlikely to bring the eruption plume to a sufficient altitude  
28 (25 km) for SO<sub>2</sub> photolysis to occur. Thus, despite the stratospheric influence of the Laki  
29 eruption, mass-independent sulfur isotope signatures in the preserved aerosols would not be  
30 expected. The situation is similar for the Cerro Hudson (1991) eruption, which had an  
31 injection height of 11 km to 16 km (Schoeberl et al., 1993). Again, given the high latitude of

1 the eruption, transport processes are likely insufficient to bring the plume ~~above 25 km to a~~  
2 ~~sufficient altitude for SO<sub>2</sub> photolysis to become a dominant process.~~

3 ~~In contrast with this are major low~~Low-latitude eruptions such as Pinatubo (1991) might  
4 behave differently. Although the initial injection of the Pinatubo eruption was probably  
5 localized below 25 km, the evolution of the plume resulted in the plume reaching altitudes of  
6 30 km or higher (Gobi et al., 1992), sufficient altitudes for SO<sub>2</sub> photolysis to play a role in the  
7 oxidation to sulfate. The largest mass-independent sulfur isotope signatures (with  $\Delta^{33}\text{S} >$   
8 1‰) observed to date are from the Samalas (1257, Lavigne et al., 2013) eruption (Lanciki et  
9 al., 2012). Evidence suggests the eruption plume from this reaction reached a minimum of 34  
10 km altitude, with a likely estimate being 43 km altitude (Lavigne et al., 2013). At this  
11 altitude, SO<sub>2</sub> photolysis would become a dominant process, and could explain why the  
12 signature from this eruption is significantly larger than the other eruptions. Thus, SO<sub>2</sub>  
13 photolysis, followed by SO oxidation to SO<sub>3</sub> (via R6), presents a consistent mechanism  
14 through which mass-independent sulfur isotope signatures can be produced and preserved in  
15 the modern, oxygenated stratosphere.

16

17 **5 Conclusions**

18 Laboratory photochemical experiments were carried out to investigate the production of  
19 mass-independent sulfur isotope effects under stratospheric conditions. For SO<sub>2</sub> photolysis in  
20 the 190 nm to 220 nm region, the magnitude of the mass-independent isotope signature  
21 increases with decreasing temperature. The isotope systematics, in particular  $\delta^{34}\text{S}$  and  $\Delta^{36}\text{S}$   
22 values, show excellent agreement with an optical self-screening model based on synthetic  
23 absorption cross sections (Lyons, 2007). SO<sub>2</sub> photoexcitation experiments show similar  
24 signatures to previous experimental studies (Whitehill and Ono, 2012; Whitehill et al., 2013),  
25 with positive  $\Delta^{33}\text{S}$  and  $\Delta^{36}\text{S}$  values, but that differ significantly from expectations based on  
26 absorption cross sections (Danielache et al., 2012).

27 The SO<sub>3</sub> (recovered as sulfate) products from SO<sub>2</sub> photolysis in the presence of molecular  
28 oxygen carry mass-independent sulfur isotope signatures, suggesting a pathway for the direct  
29 oxidation of SO to SO<sub>3</sub>. We hypothesize the  $\text{SO} + \text{O}_2 + \text{M} \rightarrow \text{SO}_3 + \text{M}$  reaction (R6) and  
30 estimate the termolecular rate constant of the reaction to be on the order of  $10^{-37} \text{ cm}^6$

1 | molecules<sup>-2</sup> s<sup>-1</sup> or faster. This is consistent with previous constraints on the maximum rate of  
2 | this reaction (Black et al., 1982).

3 | We calculated the energies of stationary points on the singlet and triplet potential energy  
4 | surfaces of SO<sub>3</sub> that are associated with the SO(<sup>3</sup>Σ<sup>-</sup>)+O<sub>2</sub>(<sup>3</sup>Σ<sub>g</sub><sup>-</sup>) asymptote at several different  
5 | levels of theory and show that reaction R6 is theoretically possible via intersystem crossing  
6 | between the singlet and triplet surfaces. We also show that the measured rate for SO + O<sub>2</sub> +  
7 | → SO<sub>2</sub> + O reaction (R5) also requires intersystem crossing between the singlet and triplet  
8 | surfaces.

9 | Depending on the rate of R6, we predict that on the order of 10% of sulfate above 25 km  
10 | altitude could be derived from the SO + O<sub>2</sub> + M channel. Given the large isotope  
11 | fractionations produced during SO<sub>2</sub> photolysis, our model can explain the source and  
12 | preservation mechanism of mass-independent sulfur isotope signatures measured in  
13 | stratospheric sulfate aerosols in polar ice samples. Furthermore, our modelexplains the  
14 | temporal evolution of δ<sup>34</sup>S and Δ<sup>33</sup>S values following major volcanic eruptions, andconstrains  
15 | the maximum altitude of the plume toabove 20 to 25 kmandabovewhen non-zero Δ<sup>33</sup>S values  
16 | are observed.

## 17 | Acknowledgements

18 | The authors would like to thank William J. Olszewski for his assistance in sulfur isotope  
19 | analysis, and support from NASA Exobiology (NNX10AR85G to S.O., and 11-EXO11-0107  
20 | to H.G.) and NSF FESD (Award 1338810 to S.O.). The authors would like to thank editor  
21 | Thomas Röckmann and reviewers Matthew Johnson and Joel Savarino for their comments.

1 **References**

2 Ahmed, M. M.: Theoretical studies on the ground and excited states of SO<sub>3</sub> triatomic  
3 molecule, *Chem. Sci. Trans.*, 2, 781-796, doi: 10.7598/cst2013.515, 2013.

4 Astholz, D. C., Glanzer, K., and Troe, J.: The spin-forbidden dissociation-recombination  
5 reaction SO<sub>3</sub> → SO<sub>2</sub>+O, *J. Chem. Phys.*, 70, 2409-2413, doi:10.1063/1.437751, 1979.

6 Baroni, M., Thiemens, M. H., Delmas, R. J., and Savarino, J.: Mass-independent sulfur  
7 isotopic compositions in stratospheric volcanic eruptions, *Science*, 315, 84-87  
8 doi:10.1126/science.1131754, 2007.

9 Baroni, M., Savarino, J., Cole-Dai, J., Rai, V. K., and Thiemens, M. H.: Anomalous sulfur  
10 isotope compositions of volcanic sulfate over the last millennium in Antarctic ice cores, *J.*  
11 *Geophys. Res. Atmos.*, 113, D20112, doi:10.1029/2008JD010185, 2008.

12 Becke, A. D., Density-functional exchange-energy approximation with correct asymptotic  
13 behavior, *Phys. Rev. A.*, 38, 3098-3100, doi:10.1103/PhysRevA.38.3098, 1988.

14 Becker, S., Braatz, C., Lindner, J., and Tiemann, E.: Investigation of the predissociation of  
15 SO<sub>2</sub>: state selective detection of the SO and O fragments, *Chem. Phys.*, 196, 275-291,  
16 doi:10.1016/0301-0104(95)00114-4, 1995.

17 Bekki, S: Oxidation of volcanic SO<sub>2</sub>: a sink for stratospheric OH and H<sub>2</sub>O, *Geophys. Res.*  
18 *Lett.*, 22, 913-916, doi:10.1029/95GL00534, 1995.

19 Bekki, S. and Pyle, J. A.: A two-dimensional modeling study of the volcanic eruption of  
20 Mount Pinatubo, *J. Geophys. Res.*, 99, 18861-18869, doi:10.1029/94JD00667, 1994.

21 Black, G., Sharpless, R. L., and Slanger, T. G.: Rate coefficients at 298 K for SO reactions  
22 with O<sub>2</sub>, O<sub>3</sub>, and NO<sub>2</sub>, *Chem. Phys. Lett.*, 90, 55-58, doi:10.1016/0009-2614(82)83324-1,  
23 1982.

24 Bluth, G. J. S., Doiron, S. D., Schnetzler, C. C., Krueger, A. J., and Walter, L. S.: Global  
25 tracking of the SO<sub>2</sub> clouds from the June, 1991 Mount Pinatubo eruptions, *Geophys. Res.*  
26 *Lett.*, 19, 151-154, doi: 10.1029/91GL02792, 1992.

27 Canfield, D. E., Raiswell, R., Westrich, J. T., Reaves, C. M., and Berner, R. A.: The use of  
28 chromium reduction in the analysis of reduced inorganic sulfur in sediments and shales,  
29 *Chem. Geol.*, 54, 149-155, doi:10.1016/0009-2541(86)90078-1, 1986.

1 Castleman, A. W., Munkelwitch, H. R., and Manowitz, B.: Isotopic studies of the sulfur  
2 component of the stratospheric aerosol layer, Tellus, 26, 222-234, doi:10.1111/j.2153-  
3 3490.1974.tb01970.x, 1974.

4 Celani, P. and Werner H.-J.: Multireference perturbation theory for large restricted and  
5 selected active space reference wave functions, J. Chem. Phys., 112, 5546-5557,doi:  
6 10.1063/1.481132, 2000.

7 Cobos, C. J., Hippel, H., and Troe, J.: Falloff curves of the recombination reaction  $O + SO +$   
8  $M \rightarrow SO_2 + M$  in a variety of bath gases, J. Phys. Chem., 89, 1778-1783, doi:  
9 10.1021/j100255a048, 1985.

10 COESA (Committee on Extension to the Standard Atmosphere): U.S. Standard Atmosphere,  
11 1976, U. S. Government Printing Office, Washington, D. C., United States of America, 1976.

12 Chase, M. W., Davies, C. A., Downey, J. R., Frurip, D. J., McDonald, R. A., and Syverud, A.  
13 N.: NIST JANAF THERMOCHEMICAL TABLES 1985 Version 1.0, Standard Reference  
14 Data Program, National Institute of Standards and Technology, Gaithersburg, MD,  
15 <http://kinetics.nist.gov/janaf/>, 1986.

16 Chung, K., Calvert, J. G., and Bottenheim, J. W.: The photochemistry of sulfur dioxide  
17 excited within its first allowed band (3130 Å) and the “forbidden” band (3700-4000 Å), Int. J.  
18 Chem. Kinet., 7, 161-182, doi: 10.1002/kin.550070202, 1975.

19 Danielache, S. O., Eskebjerg, C., Johnson, M. S., Ueno, Y., and Yoshida, N.: High-precision  
20 spectroscopy of  $^{32}S$ ,  $^{33}S$ , and  $^{34}S$  sulfur dioxide: ultraviolet absorption cross sections and  
21 isotope effects, J. Geophys. Res. Atmos., 113, D17314, doi:10.1029/2007JD009695, 2008.

22 Danielache, S. O., Hattori, S., Johnson, M. S., Ueno, Y., Nanbu, S., and Yoshida,  
23 N.: Photoabsorption cross-section measurements of  $^{32}S$ ,  $^{33}S$ ,  $^{34}S$ , and  $^{36}S$  sulfur dioxide for the  
24  $B^1B_1-X^1A_1$  absorption band, J. Geophys. Res. Atmos., 117, D24301,  
25 doi:10.1029/2012JD017464, 2012.

26 Davis, D. D.: A kinetics review of atmospheric reactions involving  $H_xO_y$  compounds, Can. J.  
27 Chem., 52, 1405-1414,doi: 10.1139/v74-213, 1974.

28 DeMore, W. B., Sander, S. P., Golden, D. M., Hampson, R. F., Kurylo, M. J., Howard, C. J.,  
29 Ravishankara, A. R., Kolb, C. E., and Molina, M. J.: Chemical kinetics and photochemical

1 data for use in stratospheric modeling, evaluation number 12, JPL Publication 97-4, Jet  
2 Propulsion Laboratory, Pasadena, California, USA, 1997.

3 Dunning, T. H.: Gaussian basis sets for use in correlated molecular calculations. I. The atoms  
4 boron through neon and hydrogen, *J. Chem. Phys.*, 90, 1007-1023, doi:  
5 10.1063/1.456153, 1989.

6 Forrest, J. and Newman, L.: Silver-110 microgram sulfate analysis for the short time  
7 resolution of ambient levels of sulfur aerosol, *Anal. Chem.*, 49, 1579-1584,  
8 doi:10.1021/ac50019a030, 1977.

9 Freeman, D. E., Yoshino, K., Esmond, J. R., and Parkinson, W. H., High resolution  
10 absorption cross section measurements of SO<sub>2</sub> at 213 K in the wavelength region 172-240 nm,  
11 *Planet. Space Sci.*, 32, 1125-1134, doi: 10.1016/0032-0633(84)90139-9, 1984.

12 Frisch, M. J., Trucks, G. W., Schlegel, H. B., Scuseria, G. E., Robb, M. A., Cheeseman, J. R.,  
13 Scalmani, G., Barone, V., Mennucci, B., Petersson, G. A., Nakatsuji, H., Caricato, M., Li, X.,  
14 Hratchian, H. P., Izmaylov, A. F., Bloino, J., Zheng, G., Sonnenberg, J. L., Hada, M., Ehara,  
15 M., Toyota, K., Fukuda, R., Hasegawa, J., Ishida, M., Nakajima, T., Honda, Y., Kitao, O.,  
16 Nakai, H., Vreven, T., Montgomery, J. A., Jr.; Peralta, J. E., Ogliaro, F., Bearpark, M., Heyd,  
17 J. J., Brothers, E., Kudin, K. N., Staroverov, V. N., Kobayashi, R., Normand, J., Raghavachari,  
18 K., Rendell, A., Burant, J. C., Iyengar, S. S., Tomasi, J., Cossi, M., Rega, N., Millam, M. J.,  
19 Klene, M., Knox, J. E., Cross, J. B., Bakken, V., Adamo, C., Jaramillo, J., Gomperts,  
20 R., Stratmann, R. E., Yazyev, O., Austin, A. J., Cammi, R., Pomelli, C., Ochterski, J. W.,  
21 Martin, R. L., Morokuma, K., Zakrzewski, V. G., Voth, G. A., Salvador, P., Dannenberg, J. J.,  
22 Dapprich, S., Daniels, A. D., Farkas, Ö., Foresman, J. B., Ortiz, J. V., Cioslowski, J., Fox, D.  
23 J.: Gaussian 09, Gaussian, Inc., Wallingford, CT, <http://www.gaussian.com/>, 2009.

24 Gobbi, G. P., Congeduti, F., and Adriani, A.: Early stratospheric effects of the Pinatubo  
25 eruption, *Geophys. Res. Lett.*, 19, 997-1000, doi:10.1029/92GL01038, 1992.

26 Goodarzi, M., Vahedpour, M., and Nazari, F.: Theoretical study on the atmospheric formation  
27 of SO<sub>x</sub>(x = 1 - 3) in the SSO(<sup>1</sup>A') and O<sub>2</sub>(<sup>3</sup>Σ<sub>g</sub><sup>-</sup>) reaction, *J. Molec. Struct. THEOCHEM*, 945,  
28 45-52, doi: 10.1016/j.theochem.2010.01.004, 2010.

29 Guo, S., Bluth, G. J. S., Rose, W. I., Watson, I. M., Prata, A. J.: Re-evaluation of SO<sub>2</sub> release  
30 of the 15 June 1991 Pinatubo eruption using ultraviolet and infrared satellite sensors,  
31 *Geochem. Geophys. Geosyst.*, 5, Q04001, doi:10.1029/2003GC000654, 2004.

1 Harris, E., Sinha, B., Hoppe, P., Crowley, J. N., Ono, S., and Foley, S.: Sulfur isotope  
2 fractionation during oxidation of sulfur dioxide: gas-phase oxidation by OH radicals and  
3 aqueous oxidation by  $\text{H}_2\text{O}_2$ ,  $\text{O}_3$ , and iron catalysis, *Atmos. Chem. Phys.*, 12, 407-424,  
4 doi:10.5194/acp-12-407-2012, 2012.

5 Harris, E., Sinha, B., Hoppe, P., and Ono, S.: High-precision measurements of  $^{33}\text{S}$  and  $^{34}\text{S}$   
6 fractionation during  $\text{SO}_2$  oxidation reveal causes of seasonality in  $\text{SO}_2$  and sulfate isotopic  
7 composition, *Environ. Sci. Tech.*, 47, 12174-12183, doi: 10.1021/es402824c, 2013.

8 Hattori, S., Schmidt, J., Johnson, M. S., Danielache, S. O., Yamada, A., Ueno, Y., and  
9 Yoshida, N.:  $\text{SO}_2$ phootoexcitation mechanism links mass-independent sulfur isotopic  
10 fractionation in cryospheric sulfate to climate impacting volcanism, *Proc. Natl. Acad. Sci.*  
11 USA, 110, 17656-17661, doi:10.1073/pnas.1213153110, 2013.

12 Jou, S. H., Shen, M. Y., Yu, C. H., and Lee, Y. P.: Isomers of  $\text{SO}_3$ : infrared absorption of  
13 OSOO in solid argon, *J. Chem. Phys.*, 104, 5745-5753, doi:10.1063/1.471335, 1996.

14 Katagiri, H., Sako, T., Hishikawa, A., Yazaki, T., Onda, K., Yamanouchi, K., and Yoshino,  
15 K.: Experimental and theoretical exploration of photodissociation of  $\text{SO}_2$  via the  $\text{C}^1\text{B}_2$  state:  
16 identification of the dissociation pathway, *J. Molec. Struct.*, 413-414, 589-614, doi:  
17 10.1016/S0022-2860(97)00199-3, 1997.

18 Knizia, G., Adler, T. B., and Werner, H.-J.: Simplified CCSD(T)-F12 methods: theory and  
19 benchmarks, *J. Chem. Phys.*, 130, 054104, doi: 10.1063/1.3054300, 2009.

20 Knowles, P. J. and Werner, H.-J.: An efficient second-order MC SCF method for long  
21 configuration expansions, *Chem. Phys. Lett.*, 115, 259-267, doi: 10.1016/0009-  
22 2614(85)80025-7, 1985.

23 Knowles, P. J. and Werner, H.-J.: An efficient method for the evaluation of coupling  
24 coefficients in configuration interaction calculations, *Chem. Phys. Lett.*, 145, 514-522, doi:  
25 10.1016/0009-2614(88)87412-8, 1988.

26 Lanciki, A. L.: Discovery of sulfur mass-independent fractionation (MIF) anomaly of  
27 stratospheric volcanic eruptions in Greenland ice cores, Ph.D. thesis, South Dakota State  
28 University, Brookings, South Dakota, United States of America, 141 pp., 2010.

1 Lanciki, A., Cole-Dai, J., Thiemens, M. H., and Savarino, J.: Sulfur isotope evidence of little  
2 or no stratospheric impact by the 1783 Laki volcanic eruption, *Geophys. Res. Lett.*, 39,  
3 L01806, doi:10.1029/2011GL050075, 2012.

4 Lavigne, F., Degeai, J. P., Komorowski, J. C., Guillet, S., Robert, V., Lahitte, P.,  
5 Oppenheimer, C., Stoffel, M., Vidal, C. M., Surono, Pratomo, I., Wassmer, P., Hajdas, I.,  
6 Hadmoko, D. S., and Belizal, E.: Source of the great A.D. 1257 mystery eruption unveiled,  
7 Samalas volcano, Rinjani Volcanic Complex, Indonesia, *Proc. Natl. Acad. Sci. USA* (Early  
8 Edition), doi: 10.1073/pnas.1307520110, 2013.

9 Lee, C., Yang, W., and Parr, R. G., Development of the Colle-Salvetti correlation-energy  
10 formula into a functional of electron density, *Phys. Rev. B.*, 37, 785-789, doi:  
11 10.1103/PhysRevB.37.785, 1988.

12 Leung, F., Colussi, A. J., and Hoffmann, M. R.: Sulfur isotopic fractionation in the gas-phase  
13 oxidation of sulfur dioxide initiated by hydroxyl radicals, *J. Phys. Chem. A*, 105, 8073-8076,  
14 doi:10.1021/jp011014+, 2001.

15 Lévêque, C., Taïeb, R., and Köppel, H.: Communication: theoretical prediction of the  
16 importance of the  ${}^3\text{B}_2$  state in the dynamics of sulfur dioxide, *J. Chem. Phys.*, 140, 091101  
17 doi:10.1063/1.4867252, 2014.

18 Lyons, J. R.: Mass-independent fractionation of sulfur isotopes by isotope-selective  
19 photodissociation of  $\text{SO}_2$ , *Geophys. Res. Lett.*, 34, L22811, doi:10.1029/2007GL031031,  
20 2007.

21 Lyons, J. R.: Photolysis of long-lived predissociative molecules as a source of mass-  
22 independent isotope fractionation: the example of  $\text{SO}_2$ , *Adv. Quant. Chem.*, 55, 57-74, doi:  
23 10.1016/S0065-3276(07)00205-5, 2008.

24 Manatt, S. L. and Lane, A. L.: A compilation of the absorption cross-sections of  $\text{SO}_2$  from  
25 106 to 403 nm, *J. Quant. Spectrosc. Radiat. Transfer*, 50, 267 - 276, doi:10.1016/0022-  
26 4073(93)90077-U, 1993.

27 Martin, J. M. L.: Heat of atomization of sulfur trioxide,  $\text{SO}_3$ : a benchmark for computational  
28 thermochemistry, *Chem. Phys. Lett.*, 310, 271-276, doi: 10.1016/S0009-2614(99)00749-6,  
29 1999.

1 Masterson, A. L., Farquhar, J., and Wing, B. A.: Sulfur mass-independent fractionation  
2 patterns in the broadband UV photolysis of sulfur dioxide: pressure and third body effects,  
3 *Earth Planet. Sci. Lett.*, 306, 253-260, doi:10.1016/j.epsl.2011.04.004, 2011.

4 Molina, L. T. and Molina, M. J.: Absolute absorption cross sections of ozone in the 185- to  
5 350-nm wavelength range, *J. Geophys. Res. Atmos.*, 91, 14501-14501, doi:  
6 10.1029/JD091iD13p14501, 1986.

7 Oduro, H., KamyshnyJr, A., Guo, W., and Farquhar, J.: Multiple sulfur isotope analysis of  
8 volatile organic sulfur compounds and their sulfonium precursors in coastal marine  
9 environments, *Marine Chem.*, 124, 78-89, doi:10.1016/j.marchem.2010.12.004, 2011.

10 Ono, S., Whitehill, A. R., and Lyons, J. R.: Contribution of isotopologue self-shielding to  
11 sulfur mass-independent fractionation during sulfur dioxide photolysis, *J. Geophys. Res.*  
12 *Atmos.*, 118, 2444-2454, doi:10.1002/jgrd.50183, 2013.

13 [Pavlov, A. A. and Kasting, J. F.: Mass-independent fractionation of sulfur isotopes in](#)  
14 [Archean sediments: Strong evidence for an anoxic Archean atmosphere. Astrobiology, 2, 27–](#)  
15 [41, doi:10.1089/153110702753621321, 2002.](#)

16 Pavlov, A. A., Mills, M. J., and Toon, O. B.: Mystery of the volcanic mass-independent sulfur  
17 isotope fractionation signature in the Antarctic ice core, *Geophys. Res. Lett.*, 32, L12816,  
18 doi:10.1029/2005GL022784, 2005.

19 [Phillips, L. F.: Absolute absorption cross sections for SO between 190 and 235 nm. J. Phys.](#)  
20 [Chem., 85, 3994 – 4000, doi: 10.1021/j150626a009, 1981.](#)

21 Ran, H., Xie, D., and Guo, H.: Theoretical studies of the C<sup>1</sup>B<sub>2</sub> absorption spectra of  
22 SO<sub>2</sub>isotopomers, *Chem. Phys. Lett.*, 439, 280-283, doi: 10.1016/j.cplett.2007.03.103, 2007.

23 Read, W. G., Froidevaux, L., and Waters, J. W.: Microwave limb sounder measurement of  
24 stratospheric SO<sub>2</sub> from the Mt. Pinatubo Volcano, *Geophys. Res. Lett.*, 20, 1299-1302, doi:  
25 10.1029/93GL00831, 1993.

26 Robock, A.: Volcanic eruptions and climate, *Rev. Geophys.*, 38(2), 191-219,  
27 doi:10.1029/1998RG000054, 2000.

28 Rottman, G. J., Woods, T. N., and McClintock, W.: SORCE solar UV irradiance results, *Adv.*  
29 *Space Res.*, 37, 201-208, doi: 10.1016/j.asr.2005.02.072, 2006.

1 Sander, S. P., Abbatt, J., Barker, J. R., Burkholder, J. B., Friedl, R. R., Golden, D. M., Huie,  
2 R. E., Kolb, C. E., Kurylo, M. J., Moortgat, G. K., Orkin, V. L., and Wine, P. H.: Chemical  
3 kinetics and photochemical data for use in atmospheric studies, evaluation no. 17, JPL  
4 Publication 10-6, Jet Propulsion Laboratory, Pasadena, California, USA,  
5 <http://jpldataeval.jpl.nasa.gov/>, 2011.

6 Savarino, J., Romero, J., Cole-Dai, J., Bekki, S., and Thiemens, M. H.: UV induced mass-  
7 independent sulfur isotope fractionation in stratospheric volcanic sulfate, *Geophys. Res. Lett.*,  
8 30, 2131, doi:10.1029/2003GL018134, 2003.

9 Schmidt, A., Thordarson, T., Oman, L. D., Robock, A., and Self, S.: Climatic impact of the  
10 long-lasting 1783 Laki eruption: inapplicability of mass-independent sulfur isotopic  
11 composition measurements, *J. Geophys. Res.*, 117, D23116, doi: 10.1029/2012JD018414,  
12 2012.

13 Schoeberl, M. R., Doiron, S. D., Lait, L. R., Newman, P. A., and Krueger, A. J.: A simulation  
14 of the Cerro Hudson SO<sub>2</sub> cloud, *J. Geophys. Res.*, 98, 2949-2955, doi:10.1029/92JD02517,  
15 1993.

16 Shemansky, D. E.: CO<sub>2</sub> extinction coefficient 1700-3000A, *J. Chem. Phys.*, 56, 1582, doi:  
17 10.1063/1.1677408, 1972.

18 Tanaka, N., Rye, D. M., Xiao, Y., and Lasaga, A. C.: Use of stable sulfur isotope systematics  
19 for evaluating oxidation reaction pathways and in-cloud scavenging of sulfur-dioxide in the  
20 atmosphere, *Geophys. Res. Lett.*, 21, 1519–1522, doi:10.1029/94GL00893, 1994.

21 Thordarson, T. and Self, S.: Atmospheric and environmental effects of the 1783-1784 Laki  
22 eruption: a review and reassessment, *J. Geophys. Res.*, 108, 4011,  
23 doi:10.1029/2001JD002042, 2003.

24 Tokue, I. and Nanbu, S.: Theoretical studies of absorption cross sections for the C<sup>1</sup>B<sub>2</sub>-X<sup>1</sup>A<sub>1</sub>  
25 system of sulfur dioxide and isotope effects, *J. Chm. Phys.*, 132, 024301, doi:  
26 10.1063/1.3277191, 2010.

27 Tsang, W. and Hampson, R. F.: Chemical kinetic database for combustion chemistry. Part I.  
28 Methane and related compounds. J. Phys. Chem. Ref. Data. 15, 1087 – 1279,  
29 doi:10.1063/1.555759, 1986.

1 Werner, H.-J., Knowles, P. J., Knizia, G., Manby, F. R., Schütz, M., Celani, P., Korona, T.,  
2 Lindh, R., Mitrushenkov, A., Rauhut, G., Shamasundar, K. R., Adler, T. B., Amos, R. D.,  
3 Bernhardsson, A., Berning, A., Cooper, D. L., Deegan, M. J. O., Dobbyn, A. J., Eckert, F., Goll,  
4 E., Hampel, C., Hesselmann, A., Hetzer, G., Hrenar, T., Jansen, G., Köppl, C., Liu, Y., Lloyd,  
5 A. W., Mata, R. A., May, A. J., McNicholas, S. J., Meyer, W., Mura, M. E., Nicklass, A.,  
6 O'Neill, D. P., Palmieri, P., Peng, D., Pflüger, K., Pitzer, R., Reiher, M., Shiozaki, T., Stoll, H.,  
7 Stone, A. J., Tarroni, R., Thorsteinsson, T., and Wang, M.: MOLPRO, version 2012.1, a  
8 package of ab initio programs, Cardiff, UK, <http://www.molpro.net>, 2012.

9 Westenberg, A. A. and Dehaas, N.: Rate of the O + SO<sub>3</sub> reaction, J. Chem. Phys., 62, 725-  
10 730, doi: 10.1063/1.430477, 1975.

11 Whitehill, A. R., and Ono, S.: Excitation band dependence of sulfur isotope mass-independent  
12 fractionation during photochemistry of sulfur dioxide using broadband light sources,  
13 Geochim. Cosmochim. Acta, 94, 238-253, doi:10.1016/j.gca.2012.06.014, 2012.

14 Whitehill, A. R., Xie, C., Hu, X., Xie, D., Guo, H., and Ono, S.: Vibronic origin of sulfur  
15 mass-independent isotope effect in photoexcitation of SO<sub>2</sub> at the implications to the early  
16 earth's atmosphere, Proc. Natl. Acad. Sci. USA, 110, 17697-17702,  
17 doi:10.1073/pnas.1306979110, 2013.

18 Xie, C., Hu, X., Zhou, L., Xie, D., and Guo, H.: *Ab initio* determination of potential energy  
19 surfaces for the first two UV absorption bands of SO<sub>2</sub>, J. Chem. Phys., 139, 014305, doi:  
20 10.1063/1.4811840, 2013.

21 Yoshino, K., Cheung, A. S. C., Esmond, J. R., Parkinson, W. H., Freeman, D. E., Guberman,  
22 S. L., Jenouvrier, A., Coquart, B., and Merienne, M. F.: Improved absorption cross-sections  
23 of oxygen in the wavelength region 205-240 nm of the Herzberg continuum, Planet. Space  
24 Sci., 36, 1469-1475, doi: 10.1016/0032-0633(88)90012-8, 1988.

25 Yoshino, K., Esmond, J. R., Cheung, A. S. C., Freeman, D. E., and Parkinson, W. H.: High  
26 resolution absorption cross sections in the transmission window of the Schumann-Runge  
27 bands and Herzberg continuum of O<sub>2</sub>, Planet. Space Sci., 40, 185-192, doi: 10.1016/0032-  
28 0633(92)90056-T, 1992.

29

1 Table 1. Summary of experiments performed

Experiment	Lamp	Filter	T / K	Bath Gas	Presented in
photolysis (temp.)	200 W D <sub>2</sub>	None	225 to 275	N <sub>2</sub>	Figures 2, 5; Table 2
photoexcitation (temp.)	150 W Xe	250 LP, H <sub>2</sub> O	225 to 275	N <sub>2</sub> /C <sub>2</sub> H <sub>2</sub>	Figure 2; Table 3
photolysis (added O <sub>2</sub> )	150 W Xe	None, 200 BP	298	N <sub>2</sub> /O <sub>2</sub>	Figures 3, 6; Tables 4, 5
photoexcitation (added O <sub>2</sub> )	150 W Xe	250 LP, 280 LP	298	N <sub>2</sub> /O <sub>2</sub>	Figure 3; Table 5

2

1 Table 2. Isotope ratios of elemental sulfur products from the SO<sub>2</sub> photolysis temperature  
2 experiments (Section 2.2)

T / K	$\delta^{33}\text{S} / \text{\textperthousand}$	$\delta^{34}\text{S} / \text{\textperthousand}$	$\delta^{36}\text{S} / \text{\textperthousand}$	$\Delta^{33}\text{S} / \text{\textperthousand}$	$\Delta^{36}\text{S} / \text{\textperthousand}$
225	103.05	191.16	349.12	8.02	-32.4
225	97.85	177.76	315.71	9.13	-35.8
250	87.19	161.31	288.97	6.61	-29.8
250	80.68	146.58	259.31	7.18	-28.9
275	72.16	132.59	236.37	5.57	-24.1
275	70.35	129.04	227.26	5.50	-25.5

3

1 Table 3. Isotope ratios of organosulfur products from the SO<sub>2</sub>photoexcitation temperature  
2 experiments (Section 2.2)

T / K	$\delta^{33}\text{S} / \text{\textperthousand}$	$\delta^{34}\text{S} / \text{\textperthousand}$	$\delta^{36}\text{S} / \text{\textperthousand}$	$\Delta^{33}\text{S} / \text{\textperthousand}$	$\Delta^{36}\text{S} / \text{\textperthousand}$
225	24.18	9.88	65.72	19.01	46.0
225	24.94	9.95	67.09	19.73	47.2
250	25.29	7.33	64.39	21.44	49.7
250	24.30	6.37	62.38	20.96	49.6
275	26.24	5.39	63.29	23.4	52.5
275	25.39	4.84	61.27	22.84	51.6

3  
4

1 Table 4. Results from experiments of  $\text{SO}_2$  photolysis in the presence of varying amounts of  $\text{O}_2$   
 2 (Section 2.3) used to estimate  $k_{\text{R}6}$  (Sections 4.3 and 4.4).

Product	$p\text{O}_2 /$ kPa	Time / ks	Yield / $\mu\text{mol S}$	$\delta^{33}\text{S} /$ ‰	$\delta^{34}\text{S} /$ ‰	$\delta^{36}\text{S} /$ ‰	$\Delta^{33}\text{S} /$ ‰	$\Delta^{36}\text{S} /$ ‰	calculated $k_{\text{R}6} /$ $\text{cm}^6 \text{molecule}^{-2} \text{s}^{-1}$
$^*\text{S}^0 - 1$	0.00	21.6		74.00	129.68	220.54	8.63	-31.9	
$^*\text{S}^0 - 2$	0.00	21.6		78.42	137.52	232.90	9.18	-34.8	
$\text{S}^0 \text{avg}$	0.00						8.91	-33.3	
$^*\text{SO}_3 - 1$	0.00	21.6	35.3	14.16	25.64	43.82	1.02	-5.2	
$^*\text{SO}_3 - 2$	0.00	21.6	28.9	11.51	21.14	36.21	0.67	-4.2	
$\text{SO}_3$	5.07	7.2	46.0	45.47	79.75	134.34	4.97	-19.5	$1.4 \times 10^{-37}$
$\text{SO}_3$	5.07	7.2	32.6	50.85	89.24	150.93	5.59	-21.6	$1.1 \times 10^{-37}$
$\text{SO}_3$	10.13	7.2	37.1	51.60	90.27	151.99	5.82	-22.5	$1.3 \times 10^{-37}$
$\text{SO}_3$	10.13	7.2	41.3	51.35	91.22	155.00	5.13	-21.5	$1.3 \times 10^{-37}$
$\text{SO}_3$	15.20	7.2	37.4	51.43	89.67	150.68	5.94	-22.6	$1.3 \times 10^{-37}$
$\text{SO}_3$	15.20	7.2	20.8	55.14	97.09	164.55	5.97	-23.4	$7.3 \times 10^{-38}$
$\text{SO}_3$	19.75	10.8	40.4	53.18	94.68	161.22	5.24	-22.2	$8.3 \times 10^{-38}$
$\text{SO}_3$	19.75	10.8	39.1	54.18	96.59	164.45	5.29	-22.7	$8.1 \times 10^{-38}$

3 \*  $\text{S}^0 - 1$  and  $\text{SO}_3 - 1$  are elemental sulfur and  $\text{SO}_3$  from the same experiment. Similarly,  $\text{S}^0 - 2$   
 4 and  $\text{SO}_3 - 2$  are elemental sulfur and  $\text{SO}_3$  from the same experiment.

5

6

1 Table 5. Results from additional experiments of SO<sub>2</sub> photolysis in the presence of O<sub>2</sub> (Section  
 2 2.3). All results are from sulfate (SO<sub>3</sub>) product. Experiments were performed at a constant  
 3 total pressure of 101.3 kPa unless marked otherwise. Filter types are: 200 BP = 200 nm  
 4 bandpass filter, 250 LP = 250 nm longpass filter, 280 LP = 280 nm longpass filter.

Filter	$p\text{SO}_2 /$ Pa	$p\text{O}_2 /$ kPa	Flow / $\text{cm}^3 \text{s}^{-1}$	Time / ks	Yield / $\mu\text{mol S}$	$\delta^{33}\text{S} /$ ‰	$\delta^{34}\text{S} /$ ‰	$\delta^{36}\text{S} /$ ‰	$\Delta^{33}\text{S} /$ ‰	$\Delta^{36}\text{S} /$ ‰
none	314.0	19.00	16.67	1.8	62.3	38.45	67.23	117.84	4.22	-12.2
none	316.6	18.99	6.67	12.8	105.7	34.71	60.89	104.88	3.69	-12.5
none	50.7	20.06	1.67	18.0	70.9	32.91	58.18	95.36	3.26	-16.2
none	50.7	20.06	1.67	10.8	41.8	37.46	67.09	112.12	3.34	-17.0
none	25.2	20.16	1.68	18.0	40.8	22.80	40.08	64.63	2.31	-12.0
none	25.2	20.16	1.68	10.8	19.3	19.59	35.15	58.01	1.61	-9.2
*none	349.9	0.20	0.29	19.8	34.0	34.02	59.04	104.90	3.92	-9.2
200 BP	316.6	18.99	6.67	67.8	86.2	47.67	89.15	162.21	2.59	-11.9
200 BP	50.7	20.06	1.67	36.0	-	35.65	65.22	111.79	2.50	-14.0
250 LP	506.5	18.23	1.67	61.2	14.9	9.40	15.97	32.53	1.19	1.9
250 LP	506.5	18.23	1.67	61.2	1.9	19.56	33.12	68.70	2.60	4.5
280 LP	316.6	18.99	6.67	86.4	6.7	3.22	4.25	9.34	1.03	1.2

5 \* Experiment performed at 7.7 kPa total pressure to test low pressure limit

1 Table 6. Comparison of asymptotic energies of SO+O<sub>2</sub> obtained on the singlet and triplet  
 2 potential energy surfaces for SO<sub>3</sub> and those obtained by the sum of two separated species. All  
 3 energies are in kJ mole<sup>-1</sup> and are relative to the SO(<sup>3</sup>Σ<sup>-</sup>) + O<sub>2</sub>(<sup>3</sup>Σ<sub>g</sub><sup>-</sup>) calculated separately in  
 4 each ab-initio method.

	B3LYP	CASSCF	CASPT2//CASSCF	UCCSD(T)F12a//B3LYP
SO( <sup>3</sup> Σ <sup>-</sup> ) + O <sub>2</sub> ( <sup>3</sup> Σ <sub>g</sub> <sup>-</sup> )	0	0	0	0
(separated)				
SO( <sup>1</sup> Δ) + O <sub>2</sub> ( <sup>3</sup> Σ <sub>g</sub> <sup>-</sup> )				
(separated)	118.78	64.60	136.36	94.98
SO( <sup>3</sup> Σ <sup>-</sup> ) + O <sub>2</sub> ( <sup>1</sup> Δ <sub>g</sub> )				
(separated)	160.83	86.57	98.28	121.55
SO( <sup>1</sup> Δ) + O <sub>2</sub> ( <sup>1</sup> Δ <sub>g</sub> )				
(separated)	279.57	151.17	234.64	216.48
SO+O <sub>2</sub> (singlet)	279.57	0.00	-6.86	217.19
SO+O <sub>2</sub> (triplet)	27.61	0.00	-6.61	122.59

5  
 6

1 Table 7. Energies for stationary points on the singlet state potential energy surface at various  
 2 ab-initio levels. The energy is relative to the  $\text{SO}({}^3\Sigma^-) + \text{O}_2({}^3\Sigma_g^-)$  asymptote and zero point  
 3 energy is not included. All energies are given in kJ mole<sup>-1</sup>.

	B3LYP	CASSCF	CASPT2//CASSCF	UCCSD(T)F12a//B3LYP
$\text{SO}_3$	-287.73	-262.92	-348.69	-411.58
cyclic-OSOO	-60.17	-50.21	-101.75	-142.72
trans-OSOO	42.09	53.72	-18.87	-17.66
cis-OSOO	19.33	35.82	-31.42	-39.08
TS1: trans-to-cis	108.95	135.14	66.32	42.76
TS2: trans-to-cyclic	62.51	69.71	3.10	0.17
TS3: cis-to-cyclic	108.95	114.18	50.42	43.26
TS4: cyclic-to- $\text{SO}_3$	82.42	69.25	56.61	70.33
$\text{SO}({}^3\Sigma^-) + \text{O}_2({}^3\Sigma_g^-)$	0.00	0.00	0.00	0.00
$\text{SO}_2({}^1\text{A}_1) + \text{O}({}^1\text{D})$	292.04	159.28	206.27	152.84

4  
 5

1 Table 8. Energies for stationary points on the triplet state potential energy surface at various  
 2 ab-initio levels. The energy is relative to the  $\text{SO}({}^3\Sigma^-) + \text{O}_2({}^3\Sigma_g^-)$  asymptote and zero point  
 3 energy is not included. All energies are given in kJ mole<sup>-1</sup>.

	B3LYP	CASSCF	CASPT2//CASSCF	UCCSD(T)F12a//B3LYP
$\text{SO}_3$	136.02	293.21	115.90	75.14
cyclic-OSOO	-70.67	12.18	-105.06	-137.07
trans-OSOO	26.40	85.81	8.70	16.53
cis-OSOO	28.58	82.09	16.82	18.49
TS1: trans-to-cis	30.42	92.72	10.79	25.44
TS2: OSOO-to-				
cyclic	96.40	125.35	67.28	67.86
$\text{SO}_2 \dots \text{O}$	23.35	-71.34	-31.55	-58.28
TS3: cyclic-to-				
$\text{SO}_2 \dots \text{O}$	25.44	-62.93	-24.81	-54.06
$\text{SO}({}^3\Sigma^-) + \text{O}_2({}^3\Sigma_g^-)$	0.00	0.00	0.00	0.00
$\text{SO}_2({}^1\text{A}_1) + \text{O}({}^3\text{P})$	26.69	-55.44	13.64	-52.93

4  
 5

1 Table 9. Reactions and rate constants included in the kinetic model of the chemistry occurring  
 2 within reaction cell. Rate constants have units of  $s^{-1}$  for first order reactions,  $cm^3\ molecule^{-1}\ s^{-1}$   
 3 for second order reactions (and effective second order reactions, denoted \*2), and  $cm^6\ molecule^{-2}\ s^{-1}$   
 4 for third order reactions.

Reaction Number	Reaction	Rate constant	Reaction Order	Source
<u>Photochemical Reactions</u>				
1	$O_2 + h\nu \rightarrow O + O$	$1.0 \times 10^{-5}$	1	Yoshino et al. (1988, 1992)
2	$O_3 + h\nu \rightarrow O + O_2$	$5.7 \times 10^{-3}$	1	Molina and Molina (1986)
3	$O_3 + h\nu \rightarrow O(^1D) + O_2$	$1.0 \times 10^{-1}$	1	Molina and Molina (1986)
4	$H_2O_2 + h\nu \rightarrow OH + OH$	$1.7 \times 10^{-3}$	1	Sander et al. (2011)
5	$HO_2 + h\nu \rightarrow O(^1D) + OH$	$1.5 \times 10^{-2}$	1	Sander et al. (2011)
6	$SO_2 + h\nu \rightarrow SO + O$	$5.2 \times 10^{-3}$	1	Manatt and Lane (1993)
7	$SO + h\nu \rightarrow S + O$	$9.7 \times 10^{-3}$	1	Phillips (1981)
<u>O<sub>x</sub> Chemistry</u>				
8	$O + O + M \rightarrow O_2 + M$	$2.5 \times 10^{-14}$	*2	Tsang and Hampson (1986)
9	$O + O_2 + M \rightarrow O_3 + M$	$1.5 \times 10^{-14}$	*2	Sander et al. (2011)
10	$O + O_3 \rightarrow O_2 + O_2$	$8.0 \times 10^{-15}$	2	Sander et al. (2011)
<u>O(^1D) Chemistry</u>				
11	$O(^1D) + O_2 \rightarrow O + O_3$	$4.0 \times 10^{-11}$	2	Sander et al. (2011)
12	$O(^1D) + O_3 \rightarrow O_2 + O_2$	$1.2 \times 10^{-10}$	2	Sander et al. (2011)
13	$O(^1D) + O_2 \rightarrow O + O + O$	$1.2 \times 10^{-10}$	2	Sander et al. (2011)
14	$O(^1D) + H_2 \rightarrow OH + H$	$1.2 \times 10^{-10}$	2	Sander et al. (2011)
15	$O(^1D) + H_2O \rightarrow OH + OH$	$2.0 \times 10^{-10}$	2	Sander et al. (2011)
16	$O(^1D) + N_2 \rightarrow O + N_2$	$3.1 \times 10^{-11}$	2	Sander et al. (2011)
17	$O(^1D) + SO_2 \rightarrow ?$	$2.2 \times 10^{-10}$	2	Sander et al. (2011)
<u>HO<sub>x</sub> Chemistry</u>				
18	$O + OH \rightarrow O_2 + H$	$3.3 \times 10^{-11}$	2	Sander et al. (2011)

- Formatted ... [1]
- Formatted ... [2]
- Formatted ... [4]
- Formatted ... [5]
- Formatted ... [6]
- Formatted ... [7]
- Formatted ... [8]
- Formatted ... [10]
- Formatted ... [12]
- Formatted ... [9]
- Formatted ... [11]
- Formatted ... [13]
- Formatted ... [15]
- Formatted ... [17]
- Formatted ... [14]
- Formatted ... [16]
- Formatted ... [18]
- Formatted ... [20]
- Formatted ... [22]
- Formatted ... [19]
- Formatted ... [21]
- Formatted ... [23]
- Formatted ... [25]
- Formatted ... [27]
- Formatted ... [24]
- Formatted ... [26]
- Formatted ... [28]
- Formatted ... [30]
- Formatted ... [32]
- Formatted ... [29]
- Formatted ... [31]
- Formatted ... [33]
- Formatted ... [35]
- Formatted ... [37]
- Formatted ... [34]
- Formatted ... [36]
- Formatted ... [38]
- Formatted ... [40]
- Formatted ... [42]
- Formatted ... [39]
- Formatted ... [41]
- Formatted ... [43]
- Formatted ... [44]
- Formatted ... [46]
- Formatted ... [48]
- Formatted ... [45]
- Formatted ... [47]
- Formatted ... [49]
- Formatted ... [51]
- Formatted ... [53]
- Formatted ... [50]
- Formatted ... [52]
- Formatted ... [54]
- Formatted ... [56]
- Formatted ... [58]

19	$O + HO_2 \rightarrow OH + O_3$	$5.9 \times 10^{-11}$	2	Sander et al. (2011)
20	$O + H_2O_2 \rightarrow OH + HO_2$	$1.8 \times 10^{-15}$	2	Sander et al. (2011)
21	$H + O_2 + M \rightarrow HO_2 + M$	$9.7 \times 10^{-13}$	*2	Sander et al. (2011)
22	$H + O_3 \rightarrow OH + O_2$	$2.9 \times 10^{-11}$	2	Sander et al. (2011)
23	$H + HO_2 \rightarrow OH + OH$	$7.2 \times 10^{-11}$	2	Sander et al. (2011)
24	$H + HO_2 \rightarrow O + H_2O$	$1.6 \times 10^{-12}$	2	Sander et al. (2011)
25	$H + HO_2 \rightarrow H_2 + O_2$	$6.9 \times 10^{-12}$	2	Sander et al. (2011)
26	$OH + O_3 \rightarrow HO_2 + O_2$	$7.3 \times 10^{-14}$	2	Sander et al. (2011)
27	$OH + H_2 \rightarrow H_2O + H$	$6.7 \times 10^{-15}$	2	Sander et al. (2011)
28	$OH + OH \rightarrow H_2O + O$	$1.8 \times 10^{-12}$	2	Sander et al. (2011)
29	$OH + OH + M \rightarrow H_2O_2 + M$	$6.4 \times 10^{-12}$	*2	Sander et al. (2011)
30	$OH + HO_2 \rightarrow H_2O + O_2$	$1.1 \times 10^{-10}$	2	Sander et al. (2011)
31	$OH + H_2O_2 \rightarrow H_2O + HO_2$	$1.8 \times 10^{-12}$	2	Sander et al. (2011)
32	$HO_2 + O_3 \rightarrow OH + O_2 + O_2$	$1.9 \times 10^{-15}$	2	Sander et al. (2011)
33	$HO_2 + HO_2 + (M) \rightarrow H_2O_2 + O_2 + (M)$	$2.6 \times 10^{-12}$	2 + *2	Sander et al. (2011)

#### SO<sub>x</sub> Chemistry

34	$O + SO_2 + M \rightarrow SO_3 + M$	$1.3 \times 10^{-11}$	*2	Sander et al. (2011)
35	$O_3 + SO_2 \rightarrow SO_3 + O_2$	$2.0 \times 10^{-22}$	2	Sander et al. (2011)
36	$OH + S \rightarrow H + SO$	$6.6 \times 10^{-11}$	2	Sander et al. (2011)
37	$OH + SO \rightarrow H + SO_2$	$8.3 \times 10^{-11}$	2	Sander et al. (2011)
38	$OH + SO_2 + M \rightarrow HOSO_2 + M$	$9.6 \times 10^{-13}$	*2	Sander et al. (2011)
39	$HO_2 + SO_2 \rightarrow OH + SO_3$	$1.0 \times 10^{-18}$	2	Sander et al. (2011)
40	$S + O_3 \rightarrow SO + O_2$	$2.3 \times 10^{-12}$	2	Sander et al. (2011)
41	$S + O_3 \rightarrow SO + O_2$	$1.2 \times 10^{-11}$	2	Sander et al. (2011)
42	$SO + O_3 \rightarrow SO_2 + O_2$	$8.0 \times 10^{-17}$	2	Sander et al. (2011)
43	$SO + O_2 + M \rightarrow SO_3 + M$	Varies	*2	Sander et al. (2011)

Formatted	... [103]
Formatted	... [105]
Formatted	... [102]
Formatted	... [104]
Formatted	... [106]
Formatted	... [108]
Formatted	... [110]
Formatted	... [107]
Formatted	... [109]
Formatted	... [111]
Formatted	... [113]
Formatted	... [115]
Formatted	... [112]
Formatted	... [114]
Formatted	... [116]
Formatted	... [118]
Formatted	... [120]
Formatted	... [117]
Formatted	... [119]
Formatted	... [121]
Formatted	... [123]
Formatted	... [125]
Formatted	... [122]
Formatted	... [124]
Formatted	... [126]
Formatted	... [128]
Formatted	... [130]
Formatted	... [127]
Formatted	... [129]
Formatted	... [131]
Formatted	... [133]
Formatted	... [135]
Formatted	... [132]
Formatted	... [134]
Formatted	... [136]
Formatted	... [138]
Formatted	... [140]
Formatted	... [137]
Formatted	... [139]
Formatted	... [141]
Formatted	... [143]
Formatted	... [145]
Formatted	... [142]
Formatted	... [144]
Formatted	... [146]
Formatted	... [148]
Formatted	... [150]
Formatted	... [147]
Formatted	... [149]
Formatted	... [151]
Formatted	... [153]
Formatted	... [155]
Formatted	... [152]
Formatted	... [154]
Formatted	... [156]
Formatted	... [158]

44	$\text{SO} + \text{O}_3 \rightarrow \text{SO}_2 + \text{O}_2$	$8.4 \times 10^{-14}$	2	Sander et al. (2011)
45	$\text{HOSO}_2 + \text{O}_3 \rightarrow \text{HO}_2 + \text{SO}_3$	$4.3 \times 10^{-13}$	2	Sander et al. (2011)
46	$\text{SO} + \text{HO}_2 \rightarrow \text{SO}_2 + \text{OH}$	$2.8 \times 10^{-11}$	2	DeMore et al. (1997)
47	$\text{SO} + \text{SO}_2 \rightarrow \text{SO}_3 + \text{S}$	$8.3 \times 10^{-16}$	2	Chung et al. (1975)
48	$\text{SO} + \text{O} + \text{M} \rightarrow \text{SO}_2 + \text{M}$	$1.3 \times 10^{-11}$	*2	Cobos et al. (1985)
49	$\text{SO} + \text{SO}_2 \rightarrow \text{SO}_2 + \text{SO}_3$	$2.0 \times 10^{-15}$	2	Chung et al. (1975)
50	$\text{S} + \text{S} + \text{M} \rightarrow \text{S}_2 + \text{M}$	$7.5 \times 10^{-14}$	*2	Pavlov and Kasting (2002)
51	$\text{SO}_2 + 2 \text{H}_2\text{O} \rightarrow \text{aerosol}$	$2.9 \times 10^{-31}$	3 (special)	Sander et al. (2011)

### Other

$k_{\text{out}}$	Exit rate from cell	$2.1 \times 10^{-2}$	1
------------------	---------------------	----------------------	---

\* Effective second order reactions based on falloff curves for  $[\text{M}] = 2.5 \times 10^{19}$  and  $\text{M} = \text{N}_2, \text{O}_2$ . See sources for additional information.

Reaction Number	Reaction	Rate constant	Reaction Order	Source
-----------------	----------	---------------	----------------	--------

### Photochemical Reactions

R4	$\text{SO}_2 + h\nu \rightarrow \text{SO} + \text{O}$	$5.2 \times 10^{-3}$	4	Manatt and Lane (1993)
R9	$\text{O}_2 + h\nu \rightarrow \text{O} + \text{O}$	$1.7 \times 10^{-6}$	4	Yoshino et al. (1988, 1992)
R10	$\text{O}_3 + h\nu \rightarrow \text{O} + \text{O}_2$	$1.1 \times 10^{-1}$	4	Molina and Molina (1986)

### O<sub>3</sub> Chemistry

R11	$\text{O} + \text{O}_2 + \text{M} \rightarrow \text{O}_2 + \text{M}$	$1.0 \times 10^{-33}$	3	Sander et al. (2011)
R12	$\text{O} + \text{O}_2 + \text{M} \rightarrow \text{O}_3 + \text{M}$	$6.0 \times 10^{-34}$	3	Sander et al. (2011)
R13	$\text{O} + \text{O}_3 \rightarrow \text{O}_2 + \text{O}_2$	$8.0 \times 10^{-15}$	2	Sander et al. (2011)

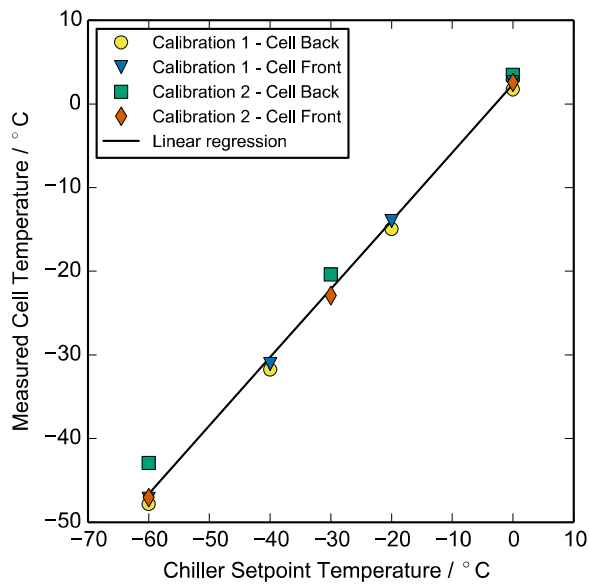
### SO<sub>x</sub> Chemistry

R5	$\text{SO} + \text{O}_2 \rightarrow \text{SO}_2 + \text{O}$	$8.0 \times 10^{-11}$	2	Sander et al. (2011)
R6	$\text{SO} + \text{O}_2 + \text{M} \rightarrow \text{SO}_3 + \text{M}$	Varies	3	
R7	$\text{SO}_2 + \text{O} + \text{M} \rightarrow \text{SO}_3 + \text{M}$	$1.3 \times 10^{-14}$	*2	Sander et al. (2011)

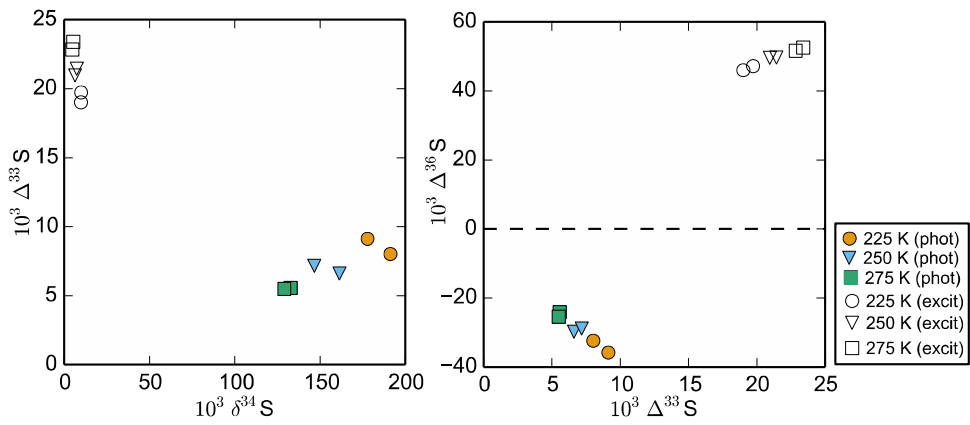
Formatted	...	[229]
Formatted	...	[231]
Formatted	...	[228]
Formatted	...	[230]
Formatted	...	[232]
Formatted	...	[234]
Formatted	...	[236]
Formatted	...	[233]
Formatted	...	[235]
Formatted	...	[237]
Formatted	...	[239]
Formatted	...	[241]
Formatted	...	[238]
Formatted	...	[240]
Formatted	...	[242]
Formatted	...	[244]
Formatted	...	[246]
Formatted	...	[243]
Formatted	...	[245]
Formatted	...	[247]
Formatted	...	[249]
Formatted	...	[251]
Formatted	...	[248]
Formatted	...	[250]
Formatted	...	[252]
Formatted	...	[254]
Formatted	...	[256]
Formatted	...	[253]
Formatted	...	[255]
Formatted	...	[257]
Formatted	...	[259]
Formatted	...	[261]
Formatted	...	[258]
Formatted	...	[260]
Formatted	...	[262]
Formatted	...	[264]
Formatted	...	[266]
Formatted	...	[263]
Formatted	...	[265]
Formatted	...	[267]
Formatted	...	[268]
Formatted	...	[269]
Formatted	...	[270]
Formatted	...	[271]
Formatted	...	[272]
Formatted	...	[273]

R8	$\text{SO} + \text{SO} \rightarrow \text{SO}_2 + \text{S}$	$8.3 \times 10^{-16}$	2	Chung et al. (1975)
R14	$\text{SO} + \text{O} + \text{M} \rightarrow \text{SO}_2 + \text{M}$	$1.3 \times 10^{-11}$	*2	Cobos et al. (1985)
R15	$\text{SO} + \text{O}_3 \rightarrow \text{SO}_2 + \text{O}_2$	$8.4 \times 10^{-14}$	2	Sander et al. (2011)
R16	$\text{S} + \text{O}_2 \rightarrow \text{SO} + \text{O}$	$2.3 \times 10^{-12}$	2	Sander et al. (2011)
R17	$\text{S} + \text{O}_3 \rightarrow \text{SO} + \text{O}_2$	$1.2 \times 10^{-11}$	2	Sander et al. (2011)
<b>Other</b>				
	$k_{\text{out}}$	Exit rate from cell	$2.1 \times 10^{-2}$	4

1 \*Effective second order reactions based on falloff curves for  $[\text{M}] = 2.5 \times 10^{19}$  and  $\text{M} = \text{N}_2, \text{O}_2$ . See  
2 sources for additional information.



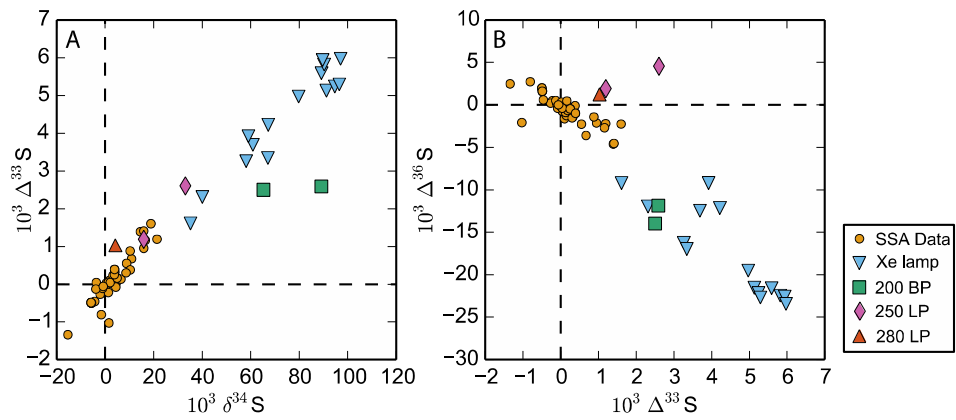
1  
2 Figure 1. Results of the temperature calibration for the temperature controlled photochemical  
3 reactor described in Section 2.1. The linear regression shown was used to calibrate the  
4 temperature within the cell based on the setpoint temperature of the chiller. The regression  
5 line is  $(T_{Cell} / ^\circ\text{C}) = 0.8160 \times (T_{Chiller} / ^\circ\text{C}) + 2.3514$ .  
6



1

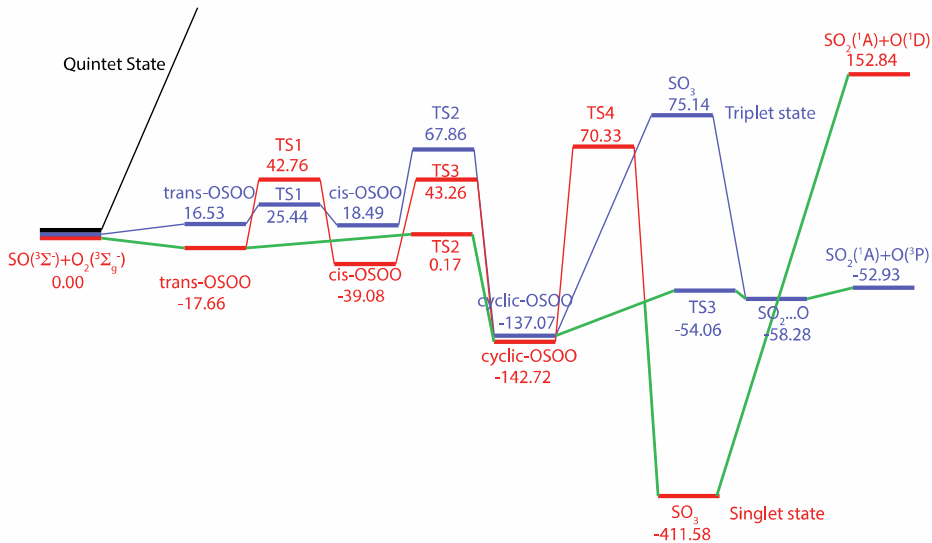
2 Figure 2. Results of the temperature experiments for  $\text{SO}_2$  photolysis and  $\text{SO}_2$  photoexcitation  
3 (Section 2.2). Results from  $\text{SO}_2$  photolysis experiments (phot) are shown in filled symbols  
4 and  $\text{SO}_2$  photoexcitation experiments (excit) are in empty symbols.

5



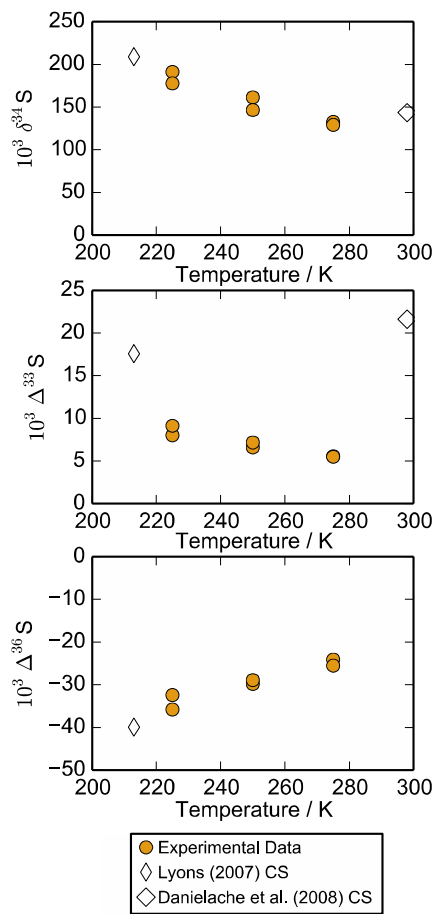
1  
2 Figure 3. Isotopic results of the  $\text{SO}_2 + \text{O}_2$  experiments described in Section 2.3, compared with  
3 stratospheric sulfate aerosol samples (SSA Data) from Savarino et al. (2003), Baroni et al.  
4 (2007, 2008), Lanciki (2010), and Lanciki et al. (2012).

5

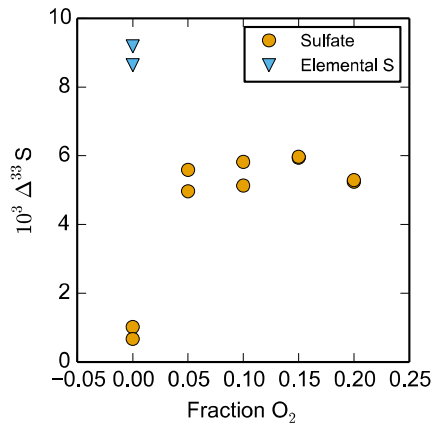


1 Figure 4. Potential energy profiles on the singlet (red) and triplet (blue) potential energy  
 2 surfaces for the  $\text{SO}_3$  system obtained using B3LYP optimization followed by UCCSD(T)-  
 3 F12a single point calculation, with the AVTZ basis set. The possible intersystem crossing  
 4 pathway is depicted by the solid green line. All energies are given in  $\text{kJ mol}^{-1}$  relative to the  
 5  $\text{SO}(^3\Sigma^-) + \text{O}_2(^3\Sigma_g^-)$  asymptote. The quintet (black) state is shown qualitatively due to its high  
 6 energy.  
 7

8  
 9



1  
2 Figure 5. Comparison of  $\text{SO}_2$  photolysis temperature experiment results with predictions from  
3 isotopologue-specific absorption cross-sections (CS).  
4

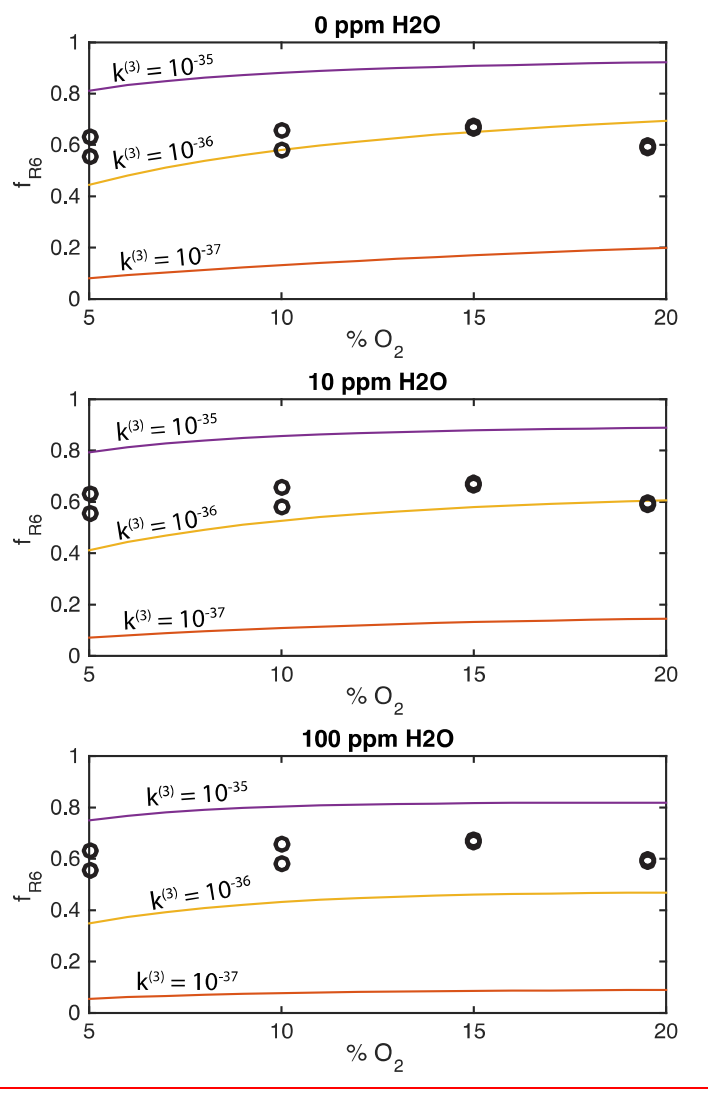


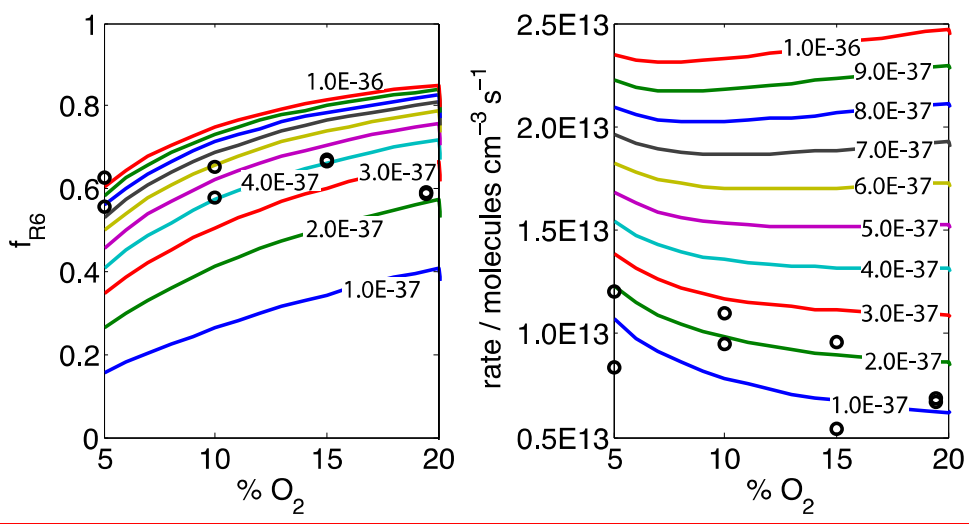
1  
2 Figure 6.  $\Delta^{33}\text{S}$  values of sulfate from the photolysis of  $\text{SO}_2$  in the presence of  $\text{O}_2$  compared  
3 with elemental sulfur and sulfate from  $\text{SO}_2$  photolysis in the absence of  $\text{O}_2$ . Conditions are  
4 described in Section 4.3 and Table 4.

5

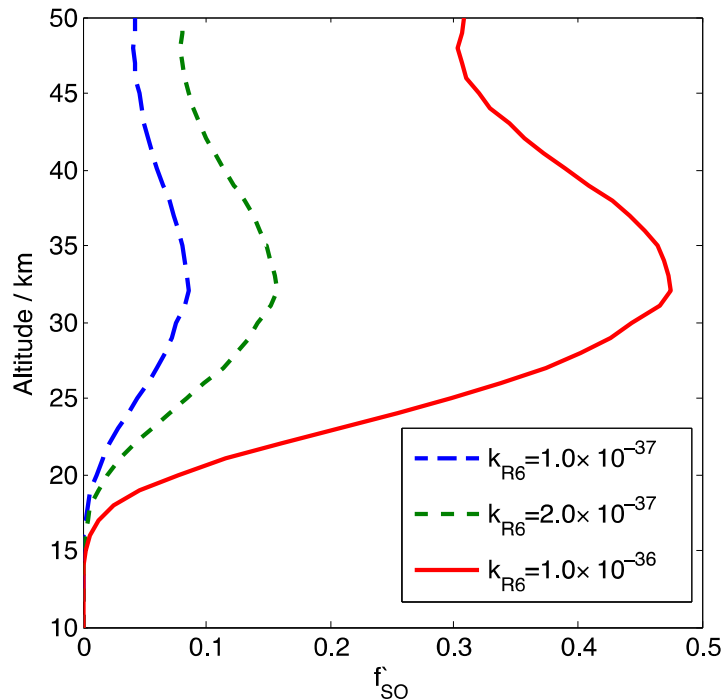


**Formatted:** Font: (Default) Times New Roman, Not Bold

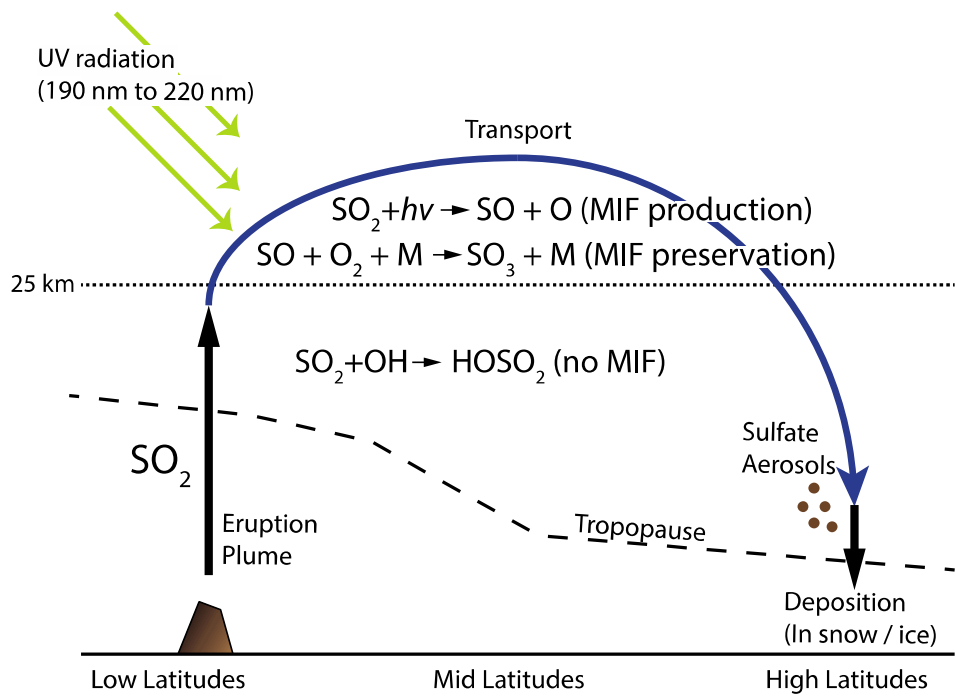




1 Figure 7. Results of kinetic model (Section 4.4, Table 9) compared to experimental data  
 2 (circles) for  $f_{R6}$  (Equation 5) versus fraction of  $SO_3$  formed from R6 in the model (left), as  
 3 well as total  $SO_3$  formation rate (right). Contours on the plot are labeled with the value of rate  
 4 constant  $k_{R6}$  input into the model for a given run. Experimental data is plotted as black  
 5 circles. The model was run for three input values of  $H_2O$  concentration: 0 ppmv (top), 10  
 6 ppmv (middle), and 100 ppmv (bottom).  
 7



1  
2 Figure 8. Fraction of sulfate derived from reaction channel R6 ( $f_{SO}$ ) as a function of altitude for  
3 different values of  $k_{R6}$ .  
4



1 Figure 9. Schematic illustration of the production and preservation of mass-independent  
 2 fractionation (MIF) in sulfur isotopes following explosive volcanic eruptions. Low latitude  
 3 eruptions such as Pinatubo (1991) inject large amounts of  $\text{SO}_2$  into the stratosphere. Through  
 4 stratospheric transport, it is brought to altitudes where  $\text{SO}_2$  photolysis can occur, producing  
 5 large MIF signatures. The product of  $\text{SO}_2$  photolysis,  $\text{SO}$ , is preserved via termolecular  
 6 reaction with  $\text{O}_2$ . The resulting  $\text{SO}_3$  forms sulfate aerosols, which are deposited at high  
 7 latitudes in polar snow and ice core records.  $\text{SO}_2$  oxidation below around 25 km is  
 8 dominantly by  $\text{OH}$ , which is a mass-dependent process.  
 9

10

12/12/2014 3:34:00 PM

12/12/2014 3:34:00 PM